Mon. Not. R. Astron. Soc. **339,** 44–62 (2003)

Imaging study of NGC 3372, the Carina nebula – I. *UBVRIJHK* photometry of Tr 14, Tr 15, Tr 16 and Car I

Mauricio Tapia,[1]★ Miguel Roth,[2] Rubén A. Vázquez[3] and Alejandro Feinstein[3]

[1]*Instituto de Astronomía UNAM, Apdo. Postal 877, 2800, Ensenada BC, Mexico*
[2]*Las Campanas Observatory, Carnegie Institution of Washington, Casilla 601, La Serena, Chile*
[3]*Facultad de Ciencias Astronómicas y Geofísicas, UNLP, IALP-CONICET, Paseo del Bosque s/n, 1900 La Plata, Argentina*

Accepted 2002 October 6. Received 2002 October 14; in original form 2002 July 23

ABSTRACT

We present the results of a large-scale imaging photometric study of the stellar population in the northern part of NGC 3372 in the *UBVRIJHK* bands with a wavelength coverage from 0.33 to 2.5 μm. The observations were made at Las Campanas Observatory. The optical CCD mosaics cover an area approximately of 32 × 22 arcmin^2 centred between the Tr 14 and Tr 16 clusters. The survey was extended to cover 12 × 12 arcmin^2 at the location of Tr 15. Near-infrared NICMOS3 mosaics covering the areas occupied by these clusters were obtained in the *JHK* photometric bands. By means of star counts in V, the centres and sizes of each cluster were redetermined yielding: Tr 14 ($r = 264$ arcsec), Tr 15 ($r = 320$ arcsec) and Tr 16 ($r = 320$ arcsec). It was confirmed that Cr 232 is not a true cluster. Multicolour optical photometry was obtained for 4152 stars. Two colour and colour-magnitude diagrams are presented and analysed for each individual cluster and compared to those of the field. We confirm the widespread variations in the dust density and also in the dust size distribution leading to widely different values of A_V and reddening laws towards Tr 14 and Tr 16. No spatial patterns were found for these variations. Spectroscopic parallaxes were computed and the results are consistent with all three clusters being at a similar distance from the Sun ($\langle d \rangle = 2.7$ kpc) but the data have shown very large scatter in both A_V and d. Analyses of the extinction-corrected colour-magnitude diagrams suggest ages between 3 and 60 million years for the stars in Tr 15 and between less than 1 and 6 million years for Tr 14 and Tr 16. A small number of infrared-excess stars were found in Tr 16 and Tr 14 but not in Tr 15. The distribution of stars in Tr 14 seen in the near-infrared suggests that this cluster is partially embedded in a molecular cloud. This molecular cloud extends towards the west reaching its highest density, marked by a CO peak emission, some three arcmin to the south-west of the nucleus of Tr 14. The rich ultraviolet field created by the Tr 14 stars ionizes most of the visible H II region in its vicinity and most of the radio H II region Car I. Evidence is found of ionization fronts leading into the molecular cloud, which appears to be 'wrapping' the Tr 14 cluster. Deep *JHK* images of the Car I region reveal the presence of an embedded stellar population illuminating a large infrared reflection nebula. It includes at least one O9–B0 star associated with an ultracompact H II region. Nebulous 2.2 μm emission from three of the mid-infrared sources in the Tr 14 region is also found.

Key words: stars: formation – H II regions – ISM: individual: NGC 3372 – open clusters and associations: general.

1 INTRODUCTION

The Great Carina nebula is not only one of the greatest celestial spectacles of the Southern skies but also a very important natural laboratory for studying the birth and evolution of the brightest and most massive stars in the Galaxy. In this huge H II region, dozens of O–B0-type stars produce a large ultraviolet (UV) radiation field which, together with strong stellar winds, interact heavily with the material in its parental giant molecular cloud.

The nebula extends more than four square degrees on the sky and, as a result of the evidently complex mass motions, it presents peculiar morphologies at all scales. These include clumps, filaments,

★E-mail: mt@astrosen.unam.mx

arcs, and all sorts of chemical, kinematical and density inhomogeneities. The gas distribution in the Carina nebula has been reported in recent years by Cox (1995, and references therein), Lee et al. (2000), Brooks et al. (2000), García & Walborn (2000), Bohigas et al. (2000) and Brooks, Storey & Whiteoak (2001).

There is mounting observational evidence that the process of massive star formation has been active for several million years and has not ceased. Recent radio CO-line observations (e.g. Cox 1995; Megeath et al. 1996; Brooks, Whiteoak & Storey 1998) together with mid-infrared (mid-IR) maps (Rathborne et al. 2002; Smith et al. 2000) of the nebula indicate that massive stars are being born in several regions within molecular condensations, located mainly to the SE and NW of the cluster Trumpler 16 (Tr 16), whose most famous member is η Carinae. It is becoming evident that the new generations of stars now being born are the result of the momentum inserted into the medium by the large-scale winds and UV radiation from the 'older' generations of stars.

In the northern part of the Carina nebula, the stellar population is dominated by the three clusters: Tr 14 and Tr 16, near the brightest part of NGC 3372, and Tr 15, a less rich stellar cluster now free of dense ambient material. The stellar population in this region has been widely studied photometrically and spectroscopically in the optical for the last three decades (Feinstein 1995 and references therein; Kaltcheva & Georgiev 1993; Vázquez et al. 1996, hereafter VBFP; DeGioia-Eastwood et al. 2001, hereafter DTWC; Carraro 2002) supplemented at near-IR wavelengths by Smith (1987) and Tapia et al. (1988). The most extensive proper motion study of the region is that of Cudworth, Martin & DeGioia-Eastwood (1993) who provided membership probabilities for nearly 600 stars in the field of Tr 14 and Tr 16. In spite of all this work, the fundamental parameters that characterize the Tr 14 and Tr 16 clusters, such as the interstellar, or more precisely, the intracluster reddening and thus, distances and ages, are still subject to controversy; see discussions by Feinstein (1995), Walborn (1995), Tapia (1995), Thé & Graafland (1995) and VBFP.

Near-IR *JHK* aperture photometry of more than 200 of the visually brightest stars in Cr 228, Tr 14, Tr 15 and Tr 16 was reported by Tapia et al. (1988) who compared their *JHK* with available *UBVRI* colours of all stars in their sample. These authors concluded that the interstellar extinction towards the cluster Tr 15, in the northern end of the Great Carina nebula, is identical to the Galactic average from 0.33 to 2.5 μm. This is not surprising, as the environment around this cluster is devoid of nebular or obscuring material.

In contrast, the other stellar clusters are characterized by highly anomalous extinction properties, especially evident at wavelengths $\lambda < 0.6$ μm, and these anomalies arise from the intracluster dust which appears to show size distributions clearly different from that of the average Galactic interstellar dust. Tapia et al. (1988) pointed out that the intracluster dust extinction properties were highly variable from star to star and that these are unrelated to location, stellar luminosity or spectral type.

Independently, Smith (1987) obtained *JHK* photometry for the 79 *K*-band brightest stars in the field of the Tr 14 and Tr 16 clusters. He complemented the data with low-resolution CVF spectra of 39 of the reddest near-IR sources. His conclusions regarding the extinction in the lines of sight toward these clusters agreed closely with those of Tapia et al. (1988) although both samples differed substantially.

By analysing the UV colours of a small sample of stars in these clusters, Tovmassian (1995) corroborated that the intracluster extinction is anomalous in this region and, with these data, he obtained an average distance of $d = 2.2$ kpc. Feinstein (1995) summarized the available photometric and spectroscopic work on the stellar population in the nebula and the results concerning the basic parameters of the open clusters: $d_{\rm Tr\,14} = 2.4$–3.9 kpc, $d_{\rm Tr\,15} = 2.4$–2.7 kpc, $d_{\rm Tr\,16} = 2.3$–3.2 kpc. The large discrepancies arise mainly by the adoption of several different values of the total to selective absorption ratio R_V. The reported ages of the clusters ranged between 3×10^6 and 6×10^6 yr. More recently, VBFP obtained a mean age of Tr 14 of 1 to 2 million years but also presented evidence that the star formation in Tr 14 has proceeded continuously for the last 5×10^6 yr.

In an attempt to extend the photometric data from the optical to the near-IR in a consistent way, here we report on the results of CCD imaging *UBVRI* photometry, covering most of the northern part of the Carina nebula, including Tr 14, Tr 15 and Tr 16 and most of the western dust lane. This is supplemented by *JHK* imaging photometry of restricted fields covering the three open clusters and the Car I CO and radio-continuum peak west of the nucleus of Tr 14. In the next section, the observations are presented. In Section 3 we describe the new photometric results. In Section 4, we discuss the size, distribution, extinction properties and population of the clusters as well as their characteristics and star-formation histories. Particular emphasis is given to several peculiar regions within the nebula which are the result of the interaction of the strong stellar winds and UV radiation with the surrounding gas and molecular material. A summary of the main conclusions is given in Section 5. Tables with the photometric results are being submitted to the Centre de Données astronomiques de Strasbourg (CDS) and will be available in electronic form through SIMBAD.

2 OBSERVATIONS

2.1 CCD imaging

CCD images were taken through $UBV(RI)_{\rm KC}$ filters with the 1.0-m telescope at Las Campanas Observatory (LCO) in 1993 March using the 1024 × 1024 pixel TEK1 CCD chip. A 3 × 2 mosaic covering 31.6×22.0 arcmin^2 was constructed from six overlapping frames for each filter and integration time. The completed mosaics are centred at $\alpha = 10^{\rm h}\,44^{\rm m}\,25^{\rm s}.6$; $\delta = -59^\circ\,36'\,35''$ (J2000) and cover most of the northern half of NGC 3372 which includes η Carinae, Tr 16, Tr 14, most of the NW dark dust lane and a fraction of the E lane. Additionally, the northernmost cluster Tr 15 was covered by single 11.7×11.7 arcmin^2 frames centred at $\alpha = 10^{\rm h}\,44^{\rm m}\,25^{\rm s}.2$; $\delta = -59^\circ\,22'\,16''$. In each position and filter, three frames were taken with exposure times 30, 120 and 1200 s in *U*; 10, 60 and 600 s in *B*; 10, 30 and 300 s in *V*; 5, 10 and 100 s in *R* and *I*.

Even with the shortest integrations, the brightest stars became saturated. The *V*-band 3-s integration mosaic containing the Tr 14 and Tr 16 clusters is shown in Fig. 1 while the corresponding individual frame centred on Tr 15 is shown in Fig. 2. The image scale was 0.70 arcsec per pixel. This was accurately computed by comparing the positions of a large number of stars in common with the recent astrometric work by DTWC, which also served to calibrate the positions of the objects. The individual CCD frames were bias subtracted and flat-field corrected in the standard way.

2.2 Near-IR imaging

JHK_s images were taken during two runs at Las Campanas Observatory. The first was with the 1.0-m (C-40) telescope in 1993 May and the second with the 2.5-m DuPont telescope in 1993 November–December. Table 1 describes the observed regions, image scale, coverages and exposure times for each observing run. For all near-IR observations, we used the LCO IR camera, which is based on

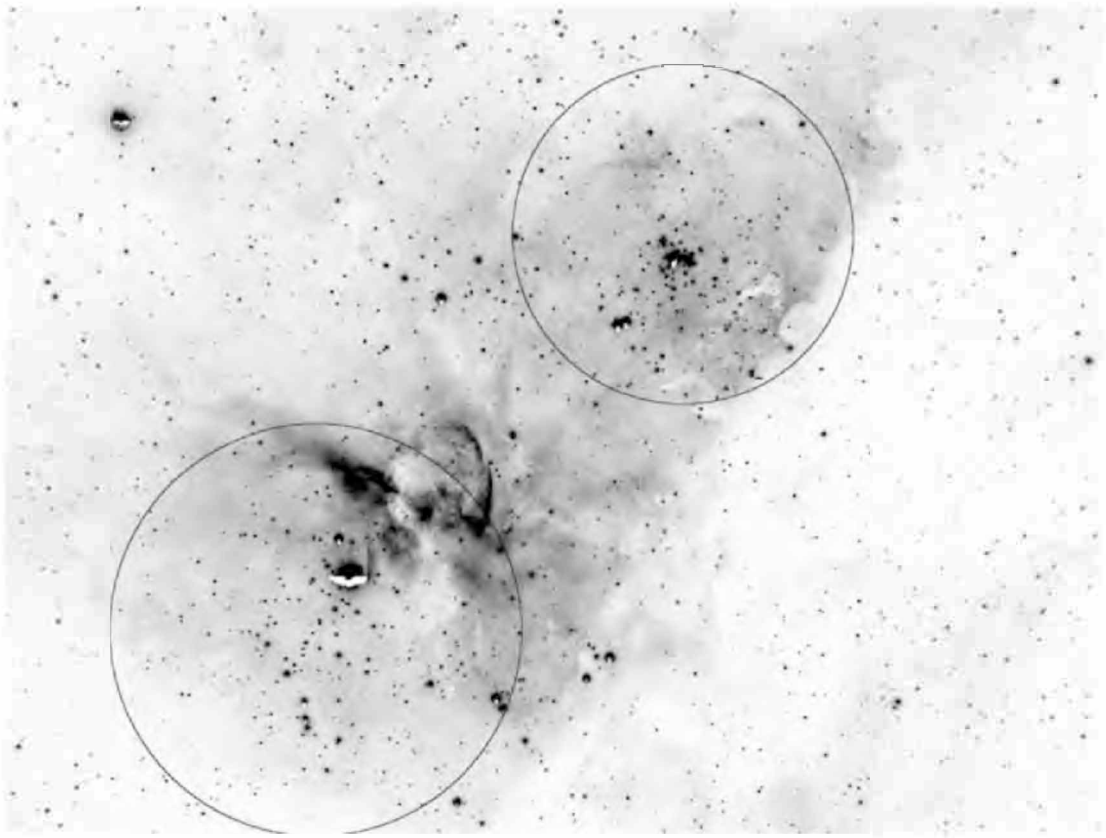

Figure 1. *R*-band short-exposure mosaic of the northern Carina nebula region containing the clusters Tr 14 and Tr 16. The area covered is 31.6×22.0 arcmin^2 centred at $\alpha = 10^{\rm h}\ 44^{\rm m}\ 25^{\rm s}.6$; $\delta = -59^\circ\ 36'\ 35''$ (J2000). North is to the top, east to the left. The circles mark the location and extension of the clusters Tr 14 and Tr 16 as derived in Section 4.1 from star counts.

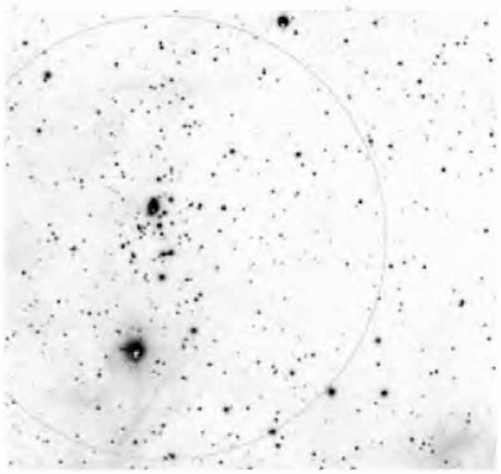

Figure 2. *R*-band short-exposure frame which includes Tr 15. The area covered is 11.7×11.7 arcmin^2 centred at $\alpha = 10^{\rm h}\ 44^{\rm m}\ 25^{\rm s}.6$; $\delta = -59^\circ\ 36'\ 35''$ (J2000). North is to the top, east to the left. The circle mark the location and extension of the cluster Tr 15 as derived in Section 4.1 from star counts.

a NICMOS3 256×256 pixel array, described in detail by Persson et al. (1992). During all observing nights, the mean point spread function (PSF) – FWHM – was less than 1 arcsec. Each frame was sky-subtracted, flat-fielded and averaged following the normal procedure. For each region and with each filter, a mosaic was constructed from the reduced overlapping individual frames. The characteristics of these mosaics are also presented in Table 1.

3 PHOTOMETRY

3.1 *UBVRI*

The photometric reductions were performed on the reduced individual images for each filter and integration setting. This was done using the DAOPHOT package (Stetson 1987) under IRAF[1] using the PSF fitting option.

Each region/filter was imaged with three integration exposures. The stars that yielded photometry within the linear region of the CCD response, and with DAOPHOT intrinsic error less than or equal to 0.02 in any pair of frames, were averaged. Naturally, the brightest stars were saturated on the long-integration time frames while the fainter stars had larger errors in the shorter integration frames and thus were not averaged. Comparing the measurements of stars in the overlapped regions, estimates of the real photometric errors were obtained. For the sake of accuracy, photometric measurements were retained only for stars brighter than the magnitude limit defined by mean intrinsic errors less than 0.04. These were the majority of the stars selected for photometry as a result of a rather conservative threshold (10σ) set to select the stars to be measured by the photometry package. Thus, the fainter stars detected on the images were neglected for the photometry, a price we paid in order to increase the accuracy of our results. It was also felt that in this way

[1]IRAF is distributed by National Optical Astronomy Observatories (NOAO) which is operated by the Association of Universities for Research in Astronomy (AURA) under contract to the National Science Foundation (NSF).

Table 1. Characteristics of near-IR observations.

Dates	Telescope	Scale arcsec per pixel	Exp. time (s)	Cluster	Central RA h m s (J2000)	Central Dec. ° ′ ″	Size arcmin^2
1993 May 5	1.0 m	0.45	120	Tr 14	10 43 35.0	−59 33 00	11.3 × 9.0
1993 May 6	1.0 m	0.45	120	Tr 15	10 44 42.7	−59 21 43	3.4 × 3.4
1993 May 5	1.0 m	0.45	120	Tr 16	10 44 50.0	−59 42 51	5.4 × 5.5
1993 Nov 30	2.5 m	0.35	30	Tr 16N	10 44 46.5	−59 36 17	8.5 × 7.4
1993 Nov 30	2.5 m	0.35	30	Tr 16S	10 44 33.0	−59 44 30	10.2 × 2.0
1993 Dec 1	2.5 m	0.35	300	Tr 14 CO	10 43 22.2	−59 34 41	0.75 × 0.75

the uncertainties introduced by a larger proportion of background star contamination were minimized.

The adopted zero points and colour equations were determined using as standard stars those in common with Feinstein and his collaborators – see Feinstein (1995) and references therein. The stars in Tr 15 (Feinstein, FitzGerald & Moffat 1980; Morrell, Garcia & Levato 1988) were given greater weight for being free of nebular contamination. To increase the range of magnitudes and colours, our calibration equations were refined by tying together our data with the CCD photometry by VBFP of the common stars in Tr 14.

In the whole area covered by these observations, the total numbers of stars measured in U, B, V, R and I were 2099, 4393, 7665, 6360 and 16 053, respectively. The brightest unsaturated stars in our images have V magnitudes between 11.5 and 12.5 while the detection completeness limits of our sample, estimated from the magnitude distributions, are $U \simeq 20.6$, $B \simeq 20.4$, $V \simeq 20.7$, $R \simeq 19.9$ and $I \simeq 20.2$. Stars as faint as 21.5 were also recorded in all filters.

Nevertheless, the numbers of stars for which reliable U–B, B–V, V–R (or V–I) colours could be measured were 1155, 2979 and 4152, respectively. This basic sample, comprised of stars with photometry in at least three colours and which forms the basis of the present investigation, has completeness limiting magnitudes of $U \simeq 18.5$, $B \simeq 18.8$, $V \simeq 17.4$, $R \simeq 16.6$ and $I \simeq 16.0$.

Fig. 3 compares our photometry with that by VBFP for more than 200 common stars in Tr 14. The mean differences ($\langle\Delta\rangle$: this work minus VBFP) and scatter (σ: standard deviation for individual measurements) for the N stars in common were

$$\langle\Delta V\rangle_{\rm VBFP} = 0.002, \sigma V_{\rm VBFP} = 0.08, (N = 288);$$

$$\langle\Delta(B{-}V)\rangle_{\rm VBFP} = 0.01, \sigma(B{-}V)_{\rm VBFP} = 0.08, (N = 242);$$

$$\langle\Delta(U{-}B)\rangle_{\rm VBFP} = 0.00, \sigma(U{-}B)_{\rm VBFP} = 0.08, (N = 93);$$

$$\langle\Delta(V{-}R)\rangle_{\rm VBFP} = 0.01, \sigma(V{-}R)_{\rm VBFP} = 0.07, (N = 221);$$

$$\langle\Delta(V{-}I)\rangle_{\rm VBFP} = 0.01, \sigma(V{-}I)_{\rm VBFP} = 0.09, (N = 159).$$

After correcting for systematic trends described by the colour equations

$$(B{-}V) = (B{-}V)_{\rm DTWC} + 0.013 V_{\rm DTWC} - 0.18$$

and

$$(U{-}B) = (U{-}B)_{\rm DTWC} + 0.013 V_{\rm DTWC} - 0.18,$$

the differences with the photometry of DTWC were found to be

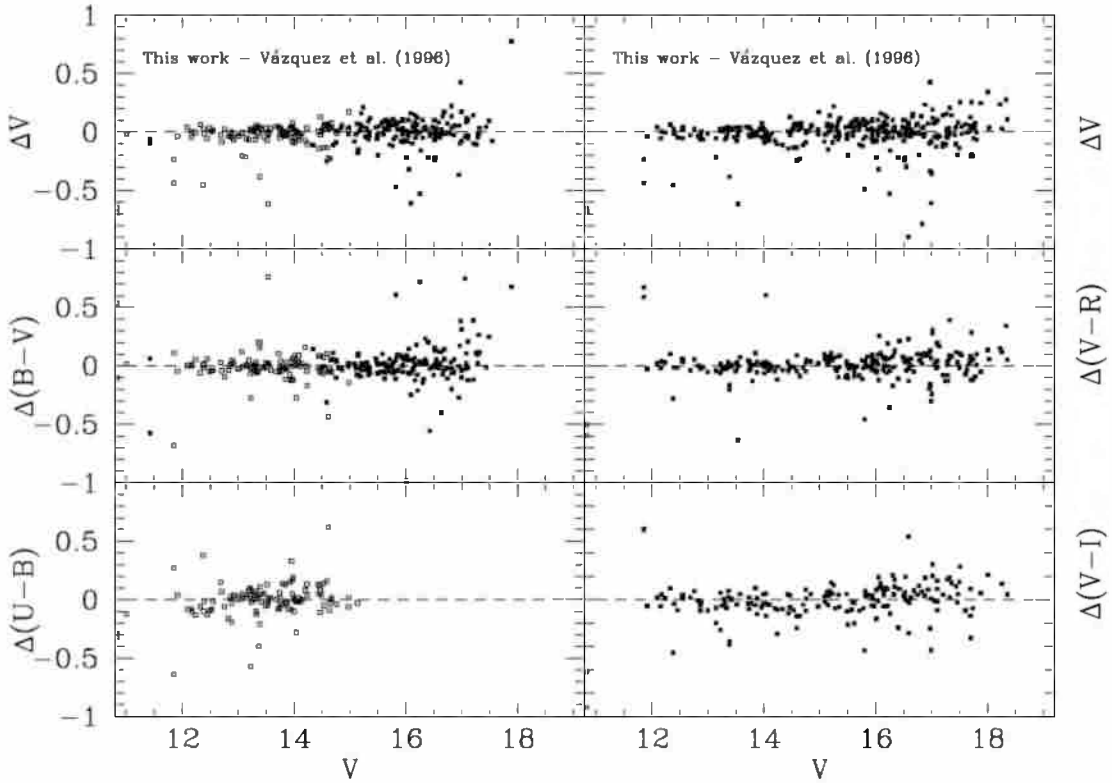

Figure 3. Comparison of the photometry presented in this work and that by VBFP. Filled squares in the left panel are stars not measured in U.

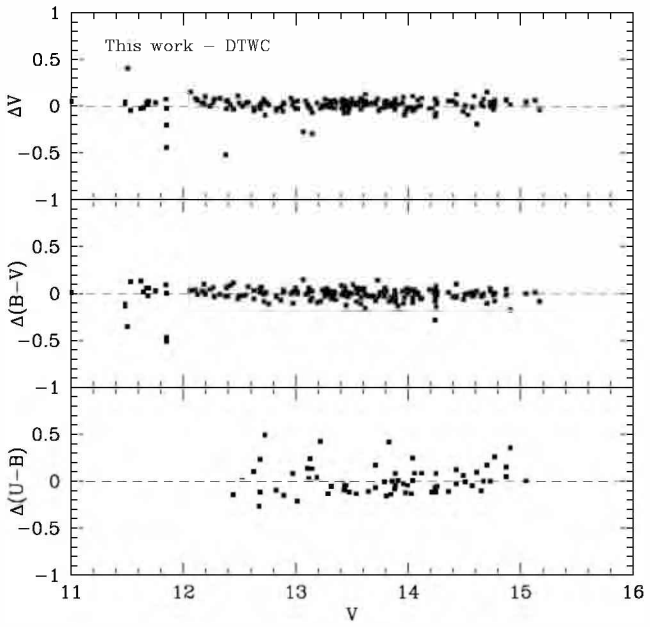

Figure 4. Comparison of the photometry presented in this work and that by DTWC.

$\langle \Delta V \rangle_{\rm DTWC} = 0.02, \sigma V_{\rm DTWC} = 0.05, (N = 173)$;

$\langle \Delta(B–V) \rangle_{\rm DTWC} = 0.00, \sigma(B–V)_{\rm DTWC} = 0.06, (N = 173)$;

$\langle \Delta(U–B) \rangle_{\rm DTWC} = -0.01, \sigma(U–B)_{\rm DTWC} = 0.11, (N = 60)$.

The comparison is illustrated graphically in Fig. 4. It should be pointed out that up to 14 stars (typically 4 per cent or less) with $|\Delta| > 0.3$ were left out for the above statistics, as these are probably variable.

The comparison with the data by Massey & Johnson (1993, hereafter MJ) shows a much larger scatter in all colours with no colour corrections (see Fig. 5):

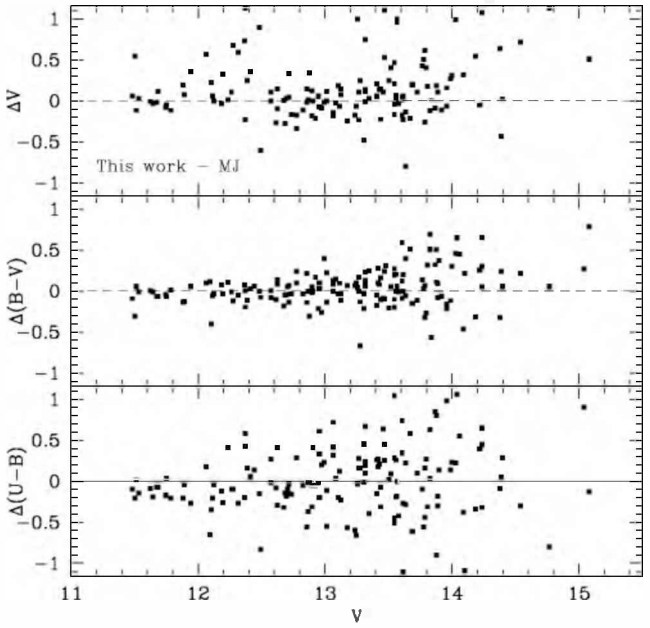

Figure 5. Comparison of the photometry presented in this work and that by MJ.

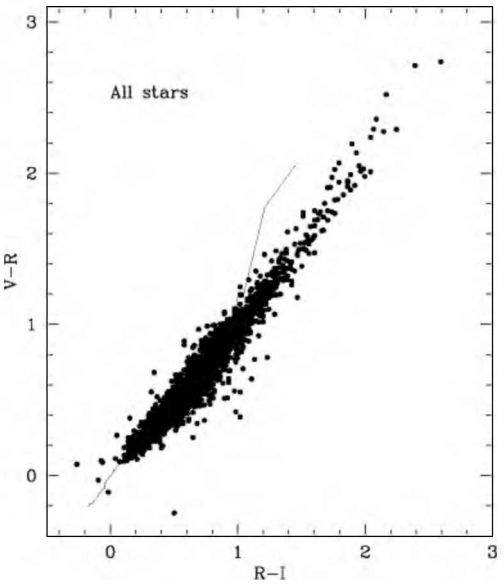

Figure 6. *V–R* versus *R–I* diagram for all stars measured in the covered area. The continuous line represents the locus of the unreddened main sequence (Schmidt-Kaler 1983).

$\langle \Delta V \rangle_{\rm MJ} = 0.03, \sigma V_{\rm MJ} = 0.19, (N = 93)$;

$\langle \Delta(B–V) \rangle_{\rm MJ} = 0.02, \sigma(B–V)_{\rm MJ} = 0.17, (N = 125)$;

$\langle \Delta(U–B) \rangle_{\rm MJ} = 0.00, \sigma(U–B)_{\rm MJ} = 0.24, (N = 76)$.

The resulting *V–R* versus *R–I* diagram for all measured stars is shown in Fig. 6. It is clear that the reddening vector follows the unreddened main sequence and that its slope is constant over the whole range of colours. In order to illustrate more precisely the photometric properties of the individual cluster parameters, the *U–B* versus *B–V*, *B–V* versus *V–I* diagrams, which yield important information about the cluster members, are presented for each cluster in Figs 7 and 8, respectively. These are discussed in Section 4.3.

3.2 *JHK*

Photometry in each of the *JHK* bands was performed on the mosaiced images with DAOPHOT (Stetson 1987) under IRAF in a similar way as that for the CCD frames as described in the previous section. Isolated stars measured by Tapia et al. (1988) and Smith (1987) were used as local standards for the photometric calibrations. PSF fits were obtained and averaged on a very large sample of isolated stars covering the mosaics with very small individual residual scatter. The mean PSF for each filter in each mosaic was the basis for the photometry. Absolute positions were measured using the astrometry of DTWC.

With a threshold level for the photometry of 4σ, 1294 stars were measured in *JHK* in the three fields (Tr 14, Tr 15 and Tr 16) and approximately half of these had counterparts measured in *VRI*. In spite of the survey images reaching similar limiting magnitudes in all filters, the number of stars detected in each filter/region was quite different, as these numbers are determined by the extinction, which is extremely variable.

The completeness limiting magnitudes are $J = H = 15.3$ and $K = 13.6$ for 1993 May and $J = H = 14.7$ and $K = 14.4$ for 1993 November. The limiting magnitudes for the deeper 1993 December images are $J = H = 17.4$ and $K = 16.5$. The typical total

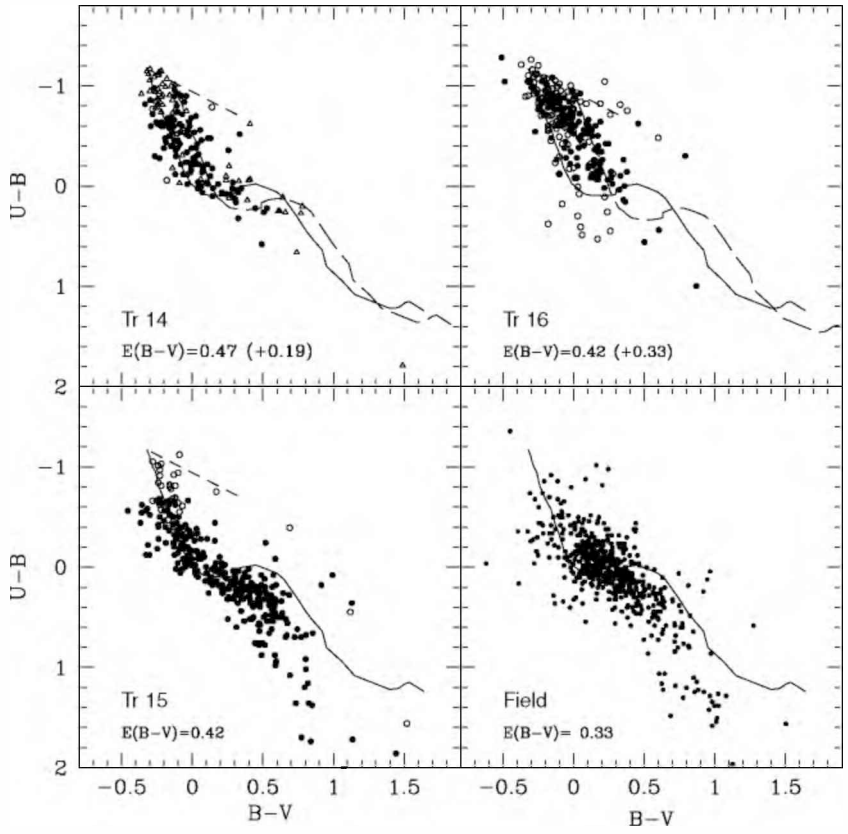

Figure 7. *U–B* versus *B–V* diagram of the stars within the areas covered by the clusters Tr 14, Tr 15 and Tr 16 as defined in Section 3.1. The stars outside the cluster boundaries are considered 'field'. The continuous lines represent the locus of the main sequence (Schmidt-Kaler 1983) corrected by the fitted excesses $E(B–V)$ quoted in each panel. For Tr 14 and Tr 16, main sequences with larger reddening corrections ($\Delta\ E(B–V)$) are also indicated by long-dashed lines. Short-dashed lines are the reddening vectors defined by $E(U–B)/E(B–V) = 0.72$. Filled circles represent the photometry from this work, open circles are aperture photometric measurements by Feinstein (1995, see references) and open triangles represent CCD photometry from VBFP for 'members' and 'probable members' of Tr 14 but not measured by us.

photometric errors, which are dominated by uncertainties in the calibration star data, are estimated to be smaller than 0.06 in all filters. The intrinsic errors and frame-to-frame scatter were always found to be smaller.

Figs 9 and 10 show, respectively, the *J–H* versus *H–K* and the *K* versus *J–K* diagrams for each cluster, while these near-IR colours are combined with the *BV* photometry in the two-colour and colour-magnitude diagrams presented in Figs 11 and 12. All these are discussed in detail in Section 4.2.

4 RESULTS AND DISCUSSION

4.1 Star counts: location and boundaries of clusters

The problem of locating and determining the extension of the clusters has been addressed before based on data from photographic plates (Turner & Moffat 1980). The present survey, nevertheless, is considerably deeper and contains a more complete and homogeneous sample to perform the star-count routine.

We have assumed that the clusters are spherical. Star counts in the *V* band were performed in a series of successive rings of increasing radii and centred at several positions around the reported nuclei of Tr 14, Tr 15, Tr 16 and Cr 232 (Turner & Moffat 1980). The fitted centre of each cluster was defined as that yielding the steepest peaked distribution and its radius was defined as that for which the excess surface density of stars becomes twice the standard deviation of the surrounding field. Fig. 13 shows the projected *V*-band star number density (the number of stars per square arcmin) up to our limiting magnitude versus radius for each of the clusters. The arrows mark their radii. The bottom panel clearly indicates that, as suggested previously, Cr 232 is not a real cluster but a condensation of bright stars in the vicinity of both Tr 14 and Tr 16. Table 2 shows the derived centres and diameters for Tr 14, Tr 15 and Tr 16 and these circles are drawn on the direct images presented in Figs 1 and 2. It is interesting to note that the boundaries determined by direct counts, regardless of the star brightness, are quite different from those defined by a number of bright stars, even to the extreme that Cr 232, sometime thought to be a separate open cluster defined by HD 93250, HD 93268 and HDE 303311 and other bright stars, is found to be void of a faint stellar population (Fig. 13) and thus cannot be considered a real cluster. Similarly, a number of other bright stars (e.g. HD 93162, CPD-59 2600) are located well beyond the southern and eastern boundaries of Tr 16. There is, nevertheless, plenty of spectroscopic and photometric evidence in the literature that most of these stars located outside the formal cluster boundaries are associated with the Carina complex and, thus, to the Tr 14 and/or Tr 16 clusters. It may be that our assumption of the sphericity of the cluster is incorrect and the centres and radii derived may then be inaccurate, but deviations from this geometry cannot be very large as we found well-defined projected number density peaks in the three clusters. There are many open clusters which are elongated (e.g. NGC 5606) and there are others

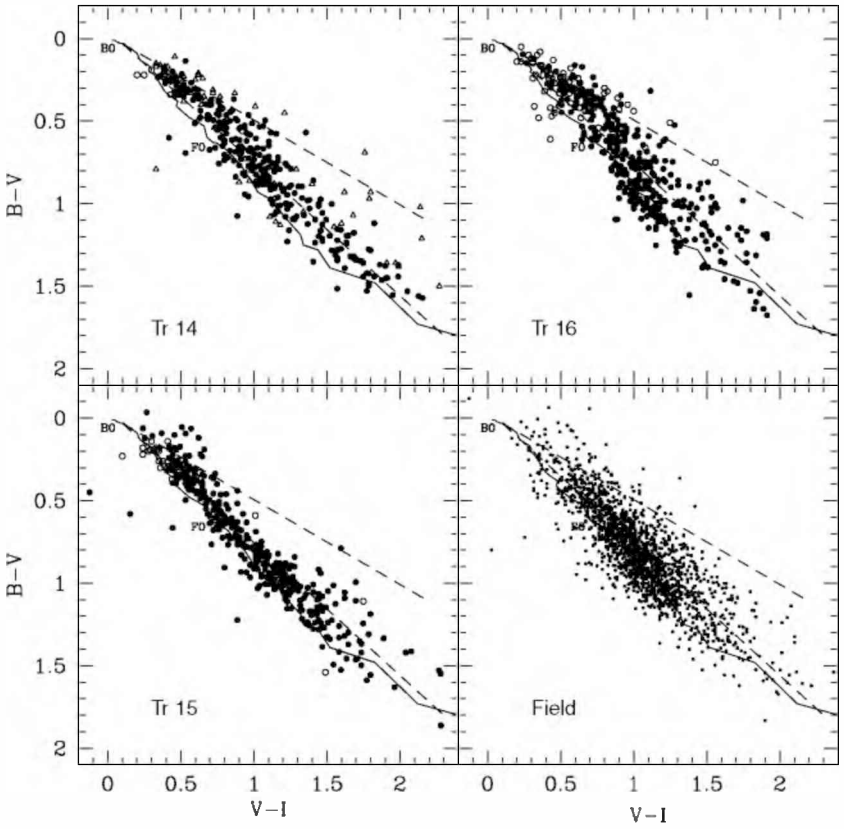

Figure 8. *B–V* versus *V–I* diagram of stars within the areas occupied by the clusters Tr 14, Tr 15 and Tr 16 and in the field. The continuous line represents the locus of the main sequence (Schmidt-Kaler 1983) corrected by one magnitude of *foreground* extinction under a 'normal reddening law' ($R_V = 3.1$; VBFP). The dashed lines are reddening vectors for O–B2 stars defined by values of $E(V–I)/E(B–V)$ of 2.03 (upper vector) typical of intracluster extinction (Tapia et al. 1988) and of 1.24 (lower vector), the 'normal' interstellar value. Symbols are as in Fig. 7.

which show a more complicated apparent morphology. Clearly, the explanation for the different apparent morphology of Tr 16 as derived from its bright or from its faint population is still unknown. Other related questions remain unanswered. Are the stars previously believed to form Cr 232 members of Tr 14 or Tr 16? Were these two clusters formed separately or were they formed as a single one?

Fig. 14 shows the position of all the stars measured in the *V*, *R* and *I* bands on our mosaic image of size 31.0 × 21.9 arcmin^2 and centred at $\alpha = 10^{\rm h}\ 44^{\rm m}\ 23^{\rm s}$, $\delta = -59^{\circ}\ 37'.0$ (J2000). The circles mark the location and extension of the clusters Tr 14 and Tr 16 as defined above and the boundaries of the *JHK* imaging surveys are also indicated. The corresponding diagram for the single frame covering Tr 15 is omitted, as this cluster does not present dust inhomogeneities.

In the Tr 14 and Tr 16 region, characterized by highly inhomogeneous extinction, the apparent shape and extension of each cluster will depend heavily on the distribution of obscuring material and on the wavelength at which the star counts are made. From a physical point of view, spherical distribution is a reasonable assumption for a rich young cluster. It can be appreciated in Fig. 1 that the sizes of the 'keyhole' dark nebulosity and several other nearby dark globules are much smaller than the area occupied by Tr 16 and should affect only marginally the statistical results of our star count exercise, as these dark features are scattered all over the cluster area. This is certainly not the case for Tr 14 which is located close to the ill-defined twisting 'boundaries' of the western 'dark lane' and with possible large-scale extinction gradients towards the southwest (Feinstein, Marraco & Muzzio 1973), in the direction of the CO peak, located 5 arcmin to the SW of the nucleus of Tr 14.

We repeated the star count exercise for the stars detected in the *K* and *H* bands in the Tr 14 region. A very asymmetric cluster is then revealed, as shown by the star position plot of Fig. 15. Under the circular cluster hypothesis, the best fit at these wavelengths was for a radius of around 100 arcsec centred at $\alpha = 10^{\rm h}\ 43^{\rm m}\ 56^{\rm s}.0$, $\delta = -59^{\circ}\ 03'\ 01''$ (J2000) with a clearly defined extension towards the SW, extending all the way to the sharp boundary of the dense dark cloud core, mapped in the CO(1–0) line by Brooks et al. (1998) and which peaks at $\alpha = 10^{\rm h}\ 43^{\rm m}\ 14^{\rm s}.6$, $\delta = -59^{\circ}\ 34'\ 45''$ (J2000). New ad-hoc boundaries of the cluster were determined by defining the area where the number density of stars, to our limiting *H* and *K* magnitudes, was higher than 28 and 16 stars per square arcmin, respectively. The mean values of the projected star densities over this area were found to be 43 (in *H*) and 30 (in *K*) stars per square arcmin, more than twice the measured projected density outside the IR-cluster area and away from the dark lanes. The newly-determined IR boundaries are marked in Fig. 15. A detailed inspection of this diagram and of the individual images indicates that the cluster ends abruptly close to the position of the sharp semicircular bright-rimmed feature clearly seen on all optical and near-IR frames and which, as pointed out by Whiteoak (1994) and Brooks et al. (2001), resembles the radio emission from the H II region. The fact that this arc-shaped emission feature defining the western dark cloud walls spatially coincide at all observed wavelengths, from 0.33 to 2.2 μm and also

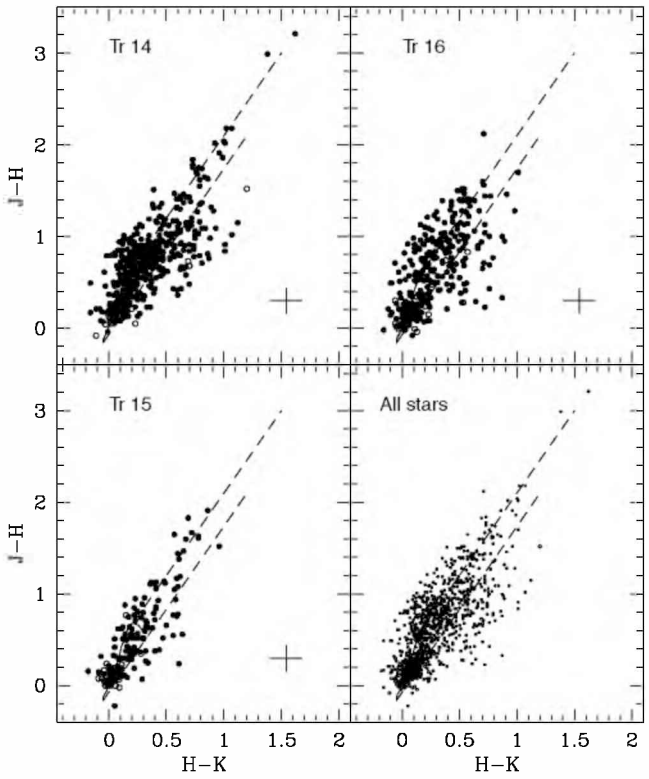

Figure 9. *J–H* versus *H–K* diagram of stars in the areas of the clusters Tr 14, Tr 15 and Tr 16. Open circles are measurements by Tapia et al. (1988). Filled circles are from this work. The continuous line represents the locus of unreddened main sequence stars (Koornneef 1983). The two parallel dashed lines represent the standard reddening vectors (of length $A_V = 20$) for late-type and early-type stars. The crosses indicate the maximum photometric errors.

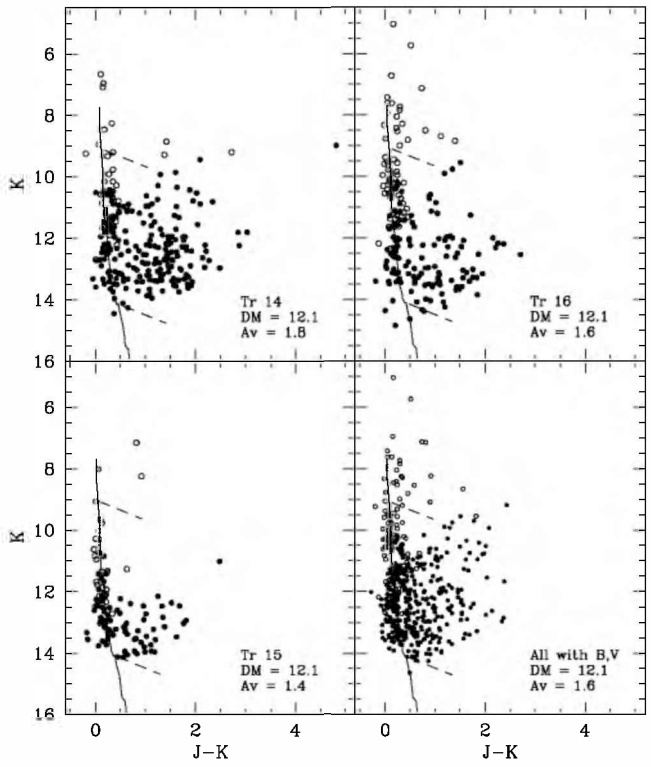

Figure 10. *K* versus *J–K* diagram for stars displaying *JHK* colours of reddened stars earlier than F5 in the areas of the clusters Tr 14, Tr 15 and Tr 16. Symbols as in Fig. 9. The continuous line represents the locus of the main sequence (Koornneef 1983; Schmidt-Kaler 1983) at distance modulus (DM) and minimum *V*-band extinction value A_V quoted in each panel. The two parallel dashed lines represent the standard reddening vectors (of length $A_V = 5$) for B0 and F0 stars.

in the 6-cm radio line and continuum, supports the suggestion that we are seeing the ionization front caused by the expansion of the H II region powered by the stars of Tr 14 into the dense molecular cloud. This also provides evidence that the physical limits of Tr 14 are determined by this interaction.

4.2 Interstellar and intracluster extinction

It is now well established that the dust extinction towards the stars in the Carina nebula is extremely variable, both in terms of variations of optical depth (measured by A_V) and, most conspicuously, of variations of shape in the extinction law (measured by $R_V = A_V/E(B–V)$). Clearly, the variable amount of absorbing grains in the line of sight determines the total extinction towards each star. Given that the star cluster members are all roughly at the same distance and the foreground extinction appears to be constant (Tapia et al. 1988), variations in A_V represent dust density fluctuations within the nebula. On the other hand, diversity in the size distribution of the *intracluster* dust grains from place to place within the nebula is the cause of the great variety of 'reddening laws' towards these stars. None of the above anomalies, mainly affecting the $E(B–V)$ colour excess index, can be attributed to the photospheric properties of the stars, as there is no correlation whatsoever between their spectral types and their extinction properties. Previous work on this subject has been reviewed extensively in the contributions by Feinstein (1995), Tapia (1995), Thé & Graafland (1995) and Tovmassian (1995) at a workshop in La Plata in late 1993.

With the present data base, the deepest and most complete to date, we are set to probe whether, for any given cluster, the A_V or the $(B–V)$-normalized extinction law $R_V = 2.22[E(V–J)/E(B–V)]$ is correlated with position, spectral type or maybe with distance. Two samples were selected for this purpose. The most reliable, but limited in number, was composed of the stars with known spectral types. The second was made up of all stars with measured *UBV* colour indices indicative of O to B9 spectral types, i.e. for which the value of $Q = (U–B) – 0.72\,(B–V) < –0.1$ (Johnson & Morgan 1953). In the latter case, following Tapia et al. (1988), intrinsic colours corresponding to their Q values were assumed for obtaining individual extinctions. The optical depth was calculated using $A_V = 1.39E(V–J)$, which is independent of variations in the extinction law (cf. Smith 1987; Tapia et al. 1988). *All* these tests yielded negative results, implying that the dust density *and* the grain size distribution do not follow any pattern within a single cluster, even towards the eastern edge of Tr 14, close to the interface with the Car I molecular cloud (see Section 4.4). The mean values and the distribution of A_V, though, do vary from cluster to cluster and this is discussed in Sections 4.3 (Table 3) and 4.4.

4.3 Distances

It is important to note that a deep photometric survey, such as that presented here, cannot provide the basis for a good distance

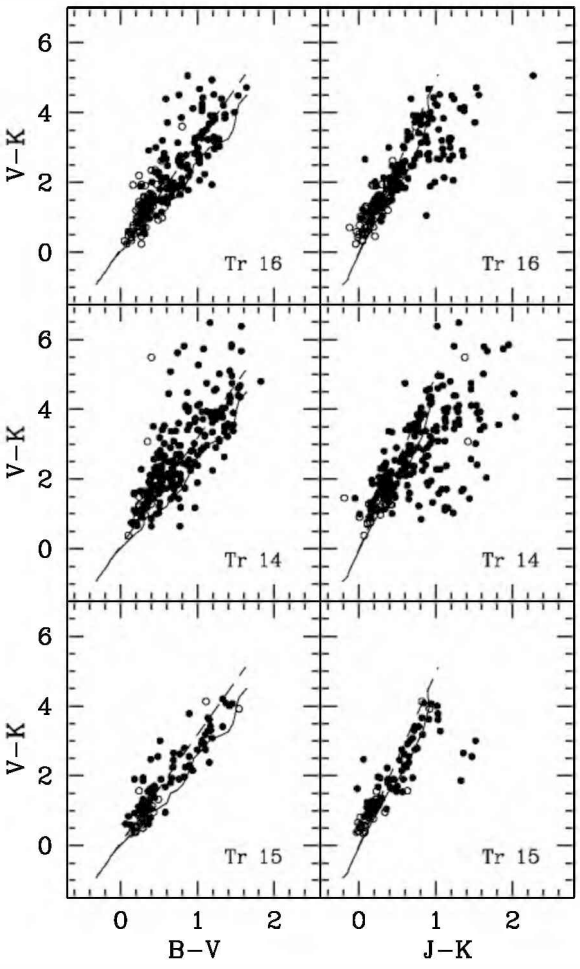

Figure 11. *V–K* versus *B–V* (left panels) and *V–K* versus *J–K* (right panels) diagrams of the stars displaying *JHK* colours of reddened stars earlier than F5 in the areas of the clusters Tr 14, Tr 15 and Tr 16. Symbols as in Fig. 9. The continuous line represents the locus occupied by unreddened main-sequence stars (Koornneef 1983; Schmidt-Kaler 1983) and the dashed line is the mean Galactic reddening vector.

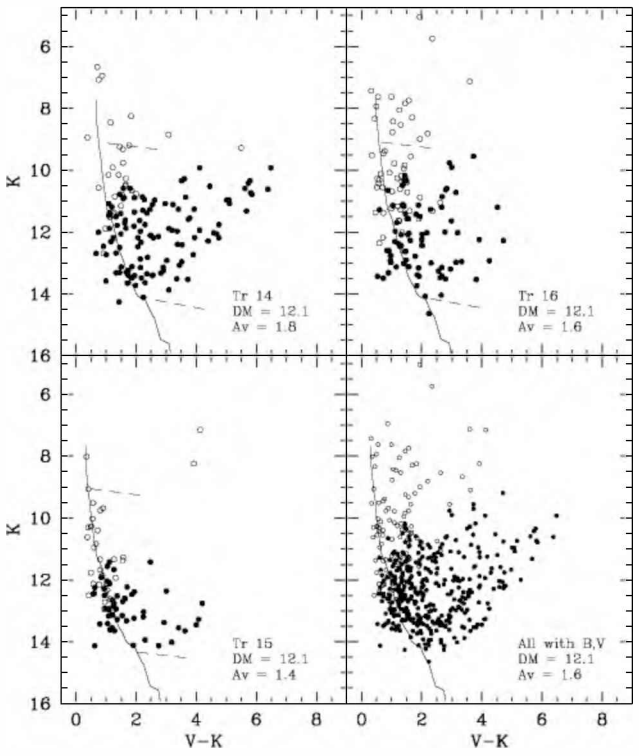

Figure 12. *K* versus *V–K* diagram of stars in the covered areas of the clusters Tr 14, Tr 15 and Tr 16. Symbols as in Fig. 9. The continuous line represents the locus occupied by the main sequence (Koornneef 1983; Schmidt-Kaler 1983) at distance modulus (DM) and minimum *V*-band extinction value A_V quoted in each panel. The two parallel dashed lines represent the standard reddening vectors (of length $A_V = 2$) for B0 and F0 stars.

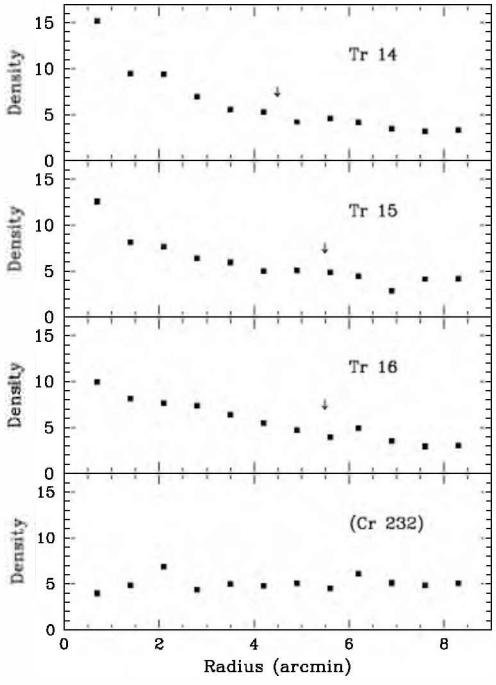

Figure 13. Projected *V*-band star number density (number of stars per square arcmin) up to our limiting magnitude versus radius for each of the clusters. The arrows mark the radii, reported in Table 2, at which the star density in the direction of each cluster becomes 2σ above the surrounding field. The presumed centre of Cr 232 was around $\alpha = 10^{\rm h}\,44^{\rm m}\,50^{\rm s}$, $\delta = -59^\circ\,33.7'$ (J2000).

determination for the Carina clusters. Uncertainties, such as age spread, undetected binarity and photometric errors, make accurate distance determination from the colour-magnitude diagrams impossible. An alternative would be to obtain statistical parallaxes. The existing data set of proper motions by Cudworth et al. (1993) includes a large number of stars in the area occupied by Tr 14 and Tr 16 and these data allow us to separate Carina complex members from those unrelated to it – field interloopers. But, unfortunately, the data fail to segregate members of different clusters. Thus, in the case of the Carina nebula clusters, the most reliable method available for distance determination is to combine individual colour excesses with accurate spectral classification (i.e. intrinsic colours and absolute magnitudes) when these are available, the so-called spectroscopic parallax method. A fair number of bright stars in the clusters Tr 14, Tr 15 and Tr 16 could be used for this procedure. Adopting the spectral types, luminosity classes and binarity information from Walborn (1973, 1982), Herbst (1976), Levato & Malaroda (1981, 1982), Morrell et al. (1988), Levato et al. (1991, 2000) and García et al. (1998), extinction-corrected distance moduli were obtained for 65 stars. Again, individual extinctions were derived assuming $R_J = A_V/E(V-J) = 1.39$ which is constant for

Table 2. Centres and radii of clusters in the V band.

Cluster	Central RA h m s (J2000)	Central dec. ° ′ ″	Radius arsec
Tr 14	10 43 55.4	−59 32 16	264
Tr 15	10 44 40.8	−59 22 10	320
Tr 16	10 45 10.6	−59 42 28	320

the general interstellar medium and for the Carina clusters (Smith 1987; Tapia et al. 1988). Intrinsic V–J colours were adopted from Kenyon & Hartmann (1995) while the absolute magnitude calibration for stars of all luminosity classes earlier than B1 was taken from Vacca, Garmany & Shull (1996) and from Schmidt-Kaler (1983) for later spectral types. The mean values and scatter for each cluster are presented in Table 3. Probably the most striking result is the large scatter in both A_V and distance moduli. It is also important to note that, although within the formal scatter, the present mean values differ from those obtained by VBFP, Carraro (2002) and Morrell et al. (1988), and these sets of values also differ significantly from each other. In the three cases, basically the same photometric and spectral data but different absolute magnitude calibrations and reddening correction methods were used. In some cases, the discrepancies are caused by variability and undetected multiplicity but clearly these factors cannot explain the differences and observed scatter. As a test, we also used the M_V calibration of Schmidt-Kaler (1983) for all stars, yielding distances within 10 per cent of those in Table 3, although Tr 15 turns out to be closer and Tr 14 and Tr 16 further away. Clearly, the problem remains unresolved.

Based on this and past results (Feinstein 1995, and references therein), we feel confident that the assumption that the three clusters are at the same distance, though different mean visual extinction, is a reasonable one. In the remainder of the discussion, a common distance of 2.63 kpc ($V_\circ - M_V = 12.1$) is assumed. As seen in the next sections, this value is consistent with the calibrated colour-magnitude diagrams of the individual clusters after allowing for the respective mean value of A_V for each cluster.

4.4 Stellar population

4.4.1 Tr 15

This cluster is located close to the northeast edge of the Carina nebula. It appears free of patches of dust. The total and intracluster mean dust absorption are significantly lower than towards the other clusters in NGC 3372. The extinction law is reported not to differ significantly from that of the Galactic average (e.g. Feinstein et al. 1980; Tapia et al. 1988). Nevertheless, the present data suggest that, on a small scale, extinction inhomogeneities in dust column density are present as confirmed by the large scatter in A_V found for the O–B9 stars with slit spectra available in the direction of Tr 15 (Table 3).

In contrast with Tr 14 and Tr 16, the absence of dense molecular material behind this cluster (cf. Brooks et al. 1998) implies a severe contamination due to background stars. This is evident from comparing the U–B versus B–V diagrams (Fig. 7) of the three clusters under study and also confronting that for stars in the areas outside the clusters' limits (the 'field'). Most of the measured OB stars in Tr 15 lie on the mean extinction-corrected main sequence while, for stars later than A0, Tr 15 resembles the 'field', implying that in this cluster the contamination of background stars mars any study of the stellar population less massive than, for example, 4 $M_\odot$. Furthermore, the B–V versus V–I diagram (Fig. 8) also presents a slight discontinuity at the locus of A0–A3 stars. The latter is caused by a change in the slope of the reddening vector which, statistically, is dominated by background dust (note that these diagrams have been corrected for foreground extinction). Therefore, a reliable analysis of the colour-magnitude diagram of this cluster must necessarily be constrained to O through B9 stars, even though the survey goes much deeper. To allow for variations in the extinction, we set a more flexible faint limit of $V = 14.8$.

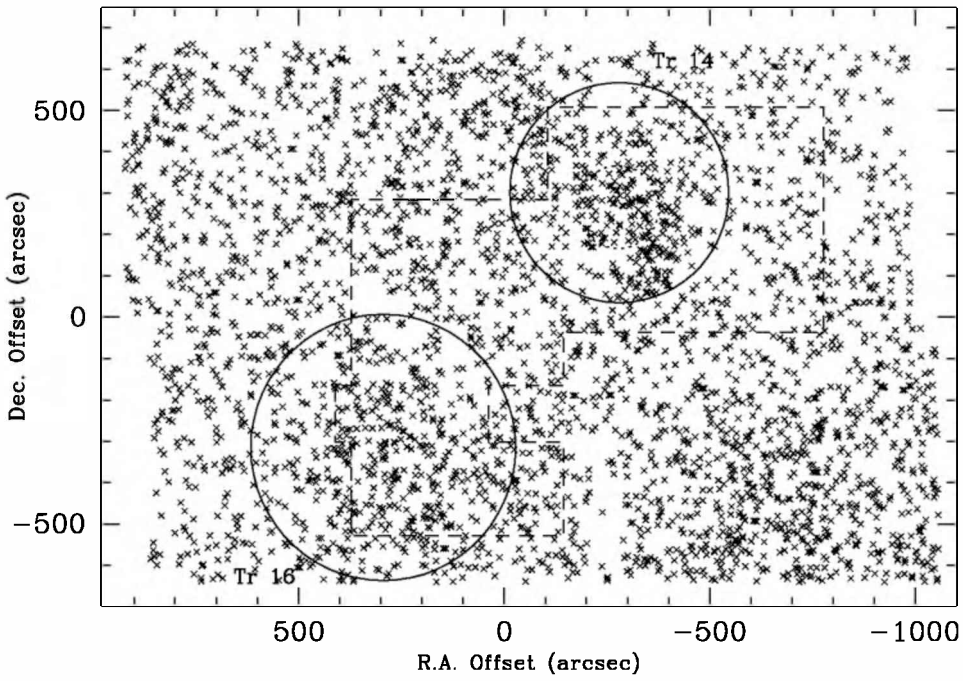

Figure 14. Positions of all the stars measured in the V, R and I bands on our mosaic image of size 31.0 × 21.9 arcmin^2 and centred at $\alpha = 10^h\,44^m\,23^s$, $\delta = -59°\,37'.0$ (J2000). The circles mark the location and extension of the clusters Tr 14 and Tr 16 as given in Table 2 and the limits of the *JHK* imaging surveys are also indicated by dashed lines.

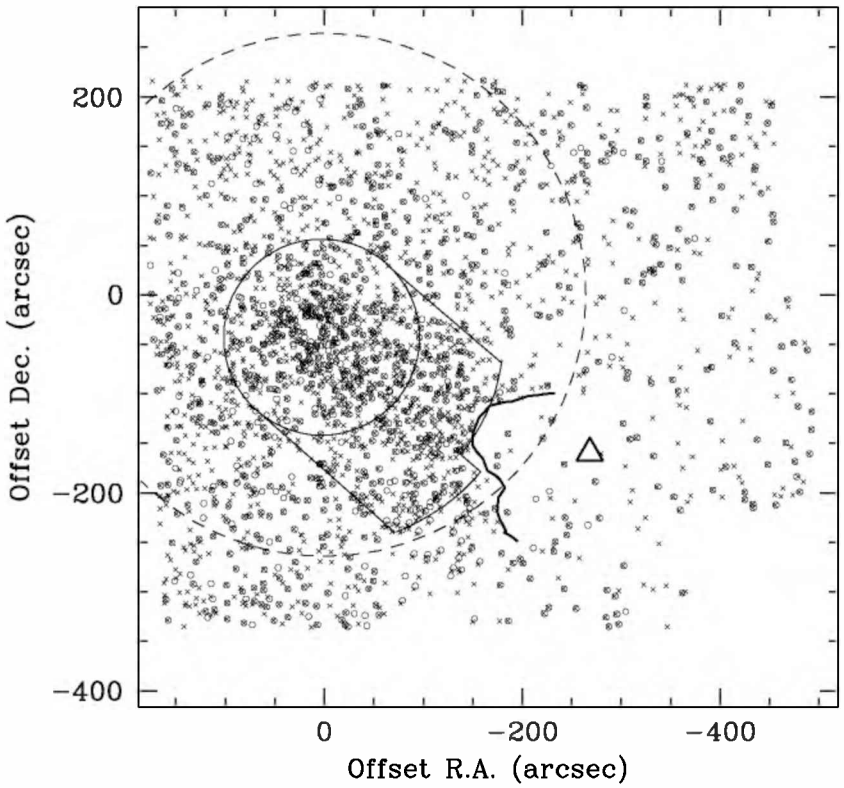

Figure 15. Position diagram of the stars detected in the K (circles) and H (crosses) bands in Tr 14 and adjacent area to the west. The dashed circle marks the boundaries of the optical cluster as given in Table 2. Note that the absence of stars near (+20, −35) is caused by saturation of several bright stars in the optical core. The thin continuous lines show the core (circle of radius 100 arcsec) and SW extension of the cluster as determined in the near-IR (see Section 4.1). The thick continuous line delineates the sharp semicircular bright-rimmed feature clearly seen on all optical and near-IR images. The triangle marks the location of the Car I CO emission peak (Whiteoak & Otrupcek 1984). The origin is at $\alpha = 10^{\rm h}\,43^{\rm m}\,55\overset{\rm s}{.}4$, $\delta = -59^{\circ}\,32'\,16''$ (J2000).

Table 3. Mean reddenings $A_V = 1.39E(V-J)$ and spectroscopic distances.

Cluster	No	DM	$\sigma_{\rm DM}$	Distance (kpc)	A_V	σ_{A_V}
Tr 14	17	12.23*	0.67*	2.8	2.52	0.44
Tr 15	17	12.34*	0.81*	2.9	1.64†	0.43†
Tr 16	32	12.02	0.57	2.5	2.06†	0.60†
All	65	12.14*	0.67*	2.7	2.08†	0.56†

*Excluding Tr 14-15 and Tr 15-21
†Excluding Tr 15-18 and Tr 16-149

Fig. 16 shows two calibrated colour-magnitude diagrams for Tr 15. The observations were corrected for the following adopted cluster parameters: distance modulus (DM), which was assumed equal for Tr 14, Tr 15 and Tr 16, and minimum $A_V = R_R E(V-R) = R_V E(B-V)$, which is the lowest value of the V-band extinction measured for the cluster members. Note that the value of R_R is 3.9 and does not vary in the interstellar medium, including the Carina nebula, while R_V is highly variable from cluster to cluster and even from star to star in NGC 3372 (Tapia et al. 1988). For this reason, the minimum $E(B-V)$ for the cluster is shown in the figure legend. The main-sequence and post-main-sequence isochrones are from Bressan et al. (1993) and the 'birthline' (B.L.) and pre-main-sequence isochrones are from Palla & Stahler (1999). We avoided applying individual extinction corrections as these imply circular arguments, such as assuming individual spectral types (intrinsic colours) to locate the stars in the HR diagram. When analysing these diagrams, care should be taken to consider differential (intracluster) extinction. For the M_V versus $V-R$ plot, a unique reddening vector applies which turns out to run almost parallel to the pre-main-sequence isochrones in this diagram. This allows us to obtain fair determinations of the ages of the clusters, using both post- and pre-main-sequence isochrones.

The presence of a significant fraction of evolved massive stars indicates that Tr 15 is the oldest of the three clusters under study. As seems to be the rule for massive young clusters, it seems impossible to assign *a single* age to Tr 15.

Most of the luminous stars lie on isochrones corresponding to ages between 3 and 40 million years. The diverging points correspond to the conspicuous stars Tr 15-28 and Tr 15-18. The latter is an O9.5I–II star (Feinstein et al. 1980; Morrell et al. 1988), suffering three magnitudes of *extra* dust absorption, A_V, relative to the cluster mean value. This is evident from its position on the $U-B$ versus $B-V$ and the $B-V$ versus $V-I$ diagrams (Figs 7 and 8). After correcting for this excess absorption, Tr 15-18 lies on the 30-Myr isochrone. The UBV colours of Tr 15-28 are consistent with a B7Ib star obscured by an extra A_V of four magnitudes (Feinstein et al. 1980) but the IR ($IJHK$) colour indices suggest that it has a late spectral type. It may well be an unresolved binary composed of a red and a blue component. As pointed out by Feinstein et al. (1980), its association with Tr 15 is in doubt. It is interesting to note that the two red supergiants in the area of Tr 15, RT Car and BO Car (even allowing for their strong variability) lie near the high-mass end of the 32-Myr and 10-Myr isochrones, respectively. This applies for the diagrams based on $B-V$ and $V-R$ (or other colour indices). Nevertheless, as statistically we expect a large number of late-type luminous field stars in this direction (along the Carina arm), no firm conclusion can be drawn about the membership of these evolved stars to Tr 15.

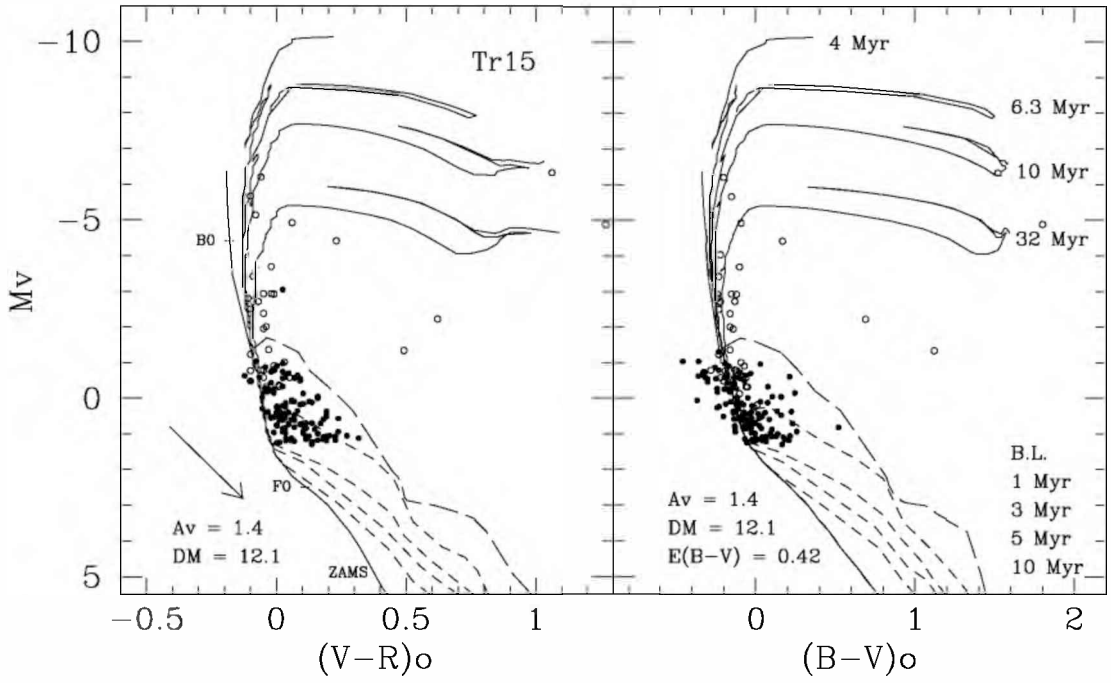

Figure 16. Calibrated colour-magnitude diagrams of Tr 15 at distance modulus (DM) and minimum extinction value A_V for stars with $V < 14.8$ to minimize confusion with the background population. The ZAMS and post-main-sequence isochrones by Bressan et al. (1993) for 4, 6.3, 10 and 32 Myr are represented by continuous lines. The birthline (B.L.) and pre-main-sequence isochrones for 1, 3, 5 and 10 Myr by Palla & Stahler (1999) are indicated by dashed lines. Note that the reddening vector (shown as an arrow) is almost parallel to the pre-main-sequence isochrones in the M_V versus $(V–R)_o$ diagram. The positions of B0V and F0V stars are indicated on the ZAMS. Open circles refer to *UBVRI* measurements by Feinstein (1995, and references therein). Filled circles are from this work and, to minimize confusion, known field stars are omitted.

Nearly a dozen other fainter stars, with *UBV* colours indicative of having B spectral types show values of A_V much higher than the majority of cluster members. In these cases, the slope of the reddening vector suggests values of $R_V > 3.5$, as in the direction of the other clusters in the nebula. No conclusions can be drawn for this cluster for the fainter stars of this subsample because of possible heavy field star contamination.

A careful examination of the *U–B* versus *B–V* diagram (Fig. 7) suggests that the most massive stars of the cluster (those with $U–B < -0.13$), have redder colour indices than the fainter ones. With the available data, it is not possible to determine whether this is caused by larger dust optical depths or variations in the extinction law which affect primarily $E(B–V)$ and $E(U–B)$.

The *JHK* survey yields a redder sample for two reasons: one is that cooler stars are more easily detected, and the second is that at these wavelengths we are able to detect stars suffering larger dust extinctions. As statistically, late-type stars constitute the majority of field stars (e.g. Jones et al. 1981), we have selected all stars in our near-IR sample which have *JHK* colours of *reddened early-type* stars (i.e. those on or to the right of the reddening vector for stars bluer than A0 in the *H–K* versus *J–H* diagram – Fig. 7). Assuming that these have colour indices negative or close to zero, the total visual extinction, $A_V = 5.8E(J–K)$, was determined for each star and the median was then obtained. For Tr 15, the median A_V was 3.4, significantly higher than the average found from the sample of (optically) bright stars with slit spectra available (Table 3). In the case of this cluster, this result has to be taken with caution, because the contamination of background blue stars may be considerable.

After individual examination, we also concluded that there is no indication that any of the few stars that appear to show near-IR excesses in the IR two-colour diagrams are associated with Tr 15 as, statistically, they are expected to be background stars.

4.4.2 Tr 14

This cluster is the richest and most highly concentrated of those that cohabit the Carina nebula. In the visible, it appears to have a radial symmetry with a radius of 3.5 pc (at $d = 2.7$ kpc; Fig. 14 and Table 2) and a mean value of extinction $A_V = 2.52$ (Table 3) with a well-defined core of some 40 arcsec (0.5 pc) in diameter. This core comprises 12 bright stars earlier than B1, including three O2–O3 stars (Walborn et al. 2002). In the near-IR (as discussed in Section 4.1), the cluster appears richer and denser than at visual wavelengths. The nucleus of the cluster extends to the southwest until it abruptly ends near the interface with the dense molecular cloud (Fig. 15). ^{12}CO maps (Brooks et al. 1998) reveal that, although the highest column density of molecular gas is close to the Car I H II radio peak a few arcmin to the west of Tr 14, the parental molecular cloud extends eastwards, extending *behind* Tr 14 as if 'wrapping' the cluster, as originally suggested by De Graauw et al. (1981).

Because of this, our sample of stars in the direction of Tr 14 is much less contaminated by field stars, as the dense molecular material behind the cluster obstructs the light of background stars even at near-IR wavelengths. This is seen in the *U–B* versus *B–V* diagram (Fig. 7) of this cluster where, up to our detection limit, only a handful of stars bluer than $U–B = 0.1$ were detected. On this diagram, most of the stars lie on the upper main-sequence locus with mean colour excesses in the range $E(B–V) = 0.47–0.66$. A

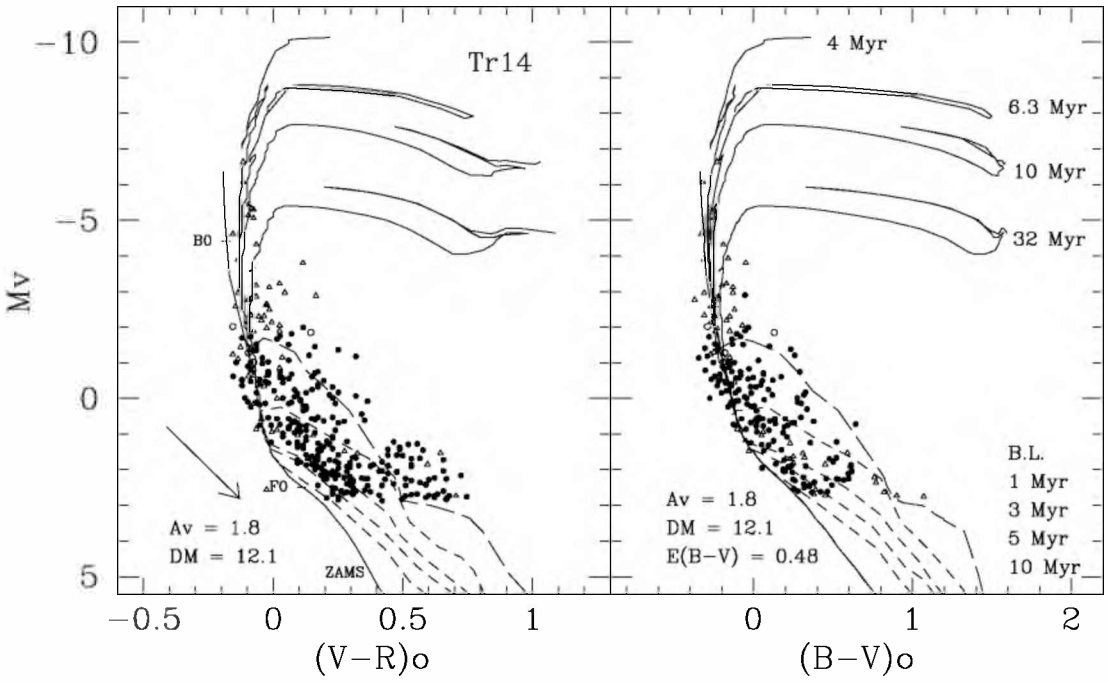

Figure 17. Calibrated colour-magnitude diagrams of Tr 14 at distance modulus (DM) and minimum extinction value A_V for stars with $V < 16.8$ to minimize confusion with the background population. Open triangles refer to measurements by VBFP. Other symbols and explanation as in Fig. 16.

few OB-type stars exhibit larger $E(B–V)$: Tr 14–65 located to the north beyond the cluster limits and three fainter stars located at the edges of dark dust cloudlets to the southeast of the cluster core.

As discussed by Tapia et al. (1988) and VBFP, the light from the members of this cluster is characterized by suffering highly anomalous absorption by intracluster dust particles. We take this fact even further, using the abnormal reddening as one basic criterion for discriminating the cluster members from the non-member stars. This can be neatly done for early-type stars in the analysis of the $B–V$ versus $V–I$ diagram (Fig. 8). Here, most of the intrinsically blue stars (spectral types earlier than F0) lie *above* the 'normal' reddening line ($E(V–I)/E(B–V) = 1.24$). This distinction is less clear for stars F0 and redder. For this reason, in the analysis of the intrinsic colour-magnitude diagram, we consider only stars earlier than F0.

Tr 14 thus appears to be emerging from the eastern and near side of the dense molecular core; see figure 5 in De Graauw et al. (1981). This geometry also explains naturally the fact that the cluster looks richer and with a modified geometry in the near-IR compared to the optical (see Section 4.1); at longer wavelengths, we see deeper into the cloud. The distribution in optical depth, measured by the individual $E(J–K)$ towards the stars in Tr 14, appears to be bimodal around the median value, which is $E(J–K) = 1.12$, implying $A_V = 6.9$. For the near-IR core, the median A_V reaches 7.3. There is no clear indication that the mean IR optical depth increases in the direction of Car I.

A relatively small number of stars show significant near-IR excesses (see $H–K$ versus $J–H$ and $V–K$ versus $J–K$ diagrams in Figs 9 and 11), the brightest being Tr 14–15, IRS 84 of Smith (1987). Comparing Smith's *JHK* photometry with that by Tapia et al. (1988) and the *UBV* colours measured independently by Feinstein et al. (1973) and VBFP, it becomes obvious that strong variations of several tenths of magnitudes at all wavelengths occur in this B7V star. IRS 75 (#157 in VBFP) displays a similar IR excess. A redder source, IRS 76 does not have an optical counterpart and its membership to the cluster cannot be tested. The case of star #54 in VBFP is also interesting as it is a bright member of the core of the cluster. Its *UVBRIJ* colour indices indicate a reddened ($A_V = 2.1$) B2 star. The *JHK* colours, on the other hand, imply a large excess at $\lambda > 2$ μm, similar to that of Tr 14–15 and IRS 75. All these stars have similar locations in the visual/IR two-colour and colour-magnitude diagrams, suggesting that they are at a similar pre-main-sequence stage. Their locations in the cluster, nevertheless, show no intercorrelation. A few other less-conspicuous sources with K-band excesses are identified and will be discussed in a future work.

The extreme dust inhomogeneities that cause large scatter in the intracluster absorption in Tr 14 make the interpretation of the colour-magnitude diagram (Fig. 17) a challenging task. The brightest stars ($M_V < -1.5$) are on or already leaving the main sequence. Given that the reddening vector (e.g. in the V versus $V–R$ diagram, Fig. 17) goes roughly perpendicular to the 'post-main-sequence' isochrones for those stars, assigning their ages is, at the least, inaccurate. In order to overcome this problem, VBFP located a number of these bright, massive stars on the intrinsic $H–R$ magnitude diagram based on their two-dimensional spectral classifications. They estimated the ages of the most massive stars in Tr 14 to be in the range 1–5 × 10^6 yr. Our new data give information about lower mass stars. Ignoring the bunch of stars with $M_V = 1$–3 and $V - R > 0.4$ and the few above the birthline which are undoubtedly field stars, we find that the ages of the F0 to B8 stars, where the reddening vector $V–R$ is *parallel* to the 'pre-main-sequence' isochrones, range from less than 1 to 5 × 10^6 yr, in agreement with VBFP and DTWC. We thus conclude that the formation of Tr 14 stars of *all* masses (down to our limit of 2 $M_\odot$) started 5 × 10^6 yr ago, proceeding continuously until less than one million years ago.

As expected for a cluster this young, a number of stars that have not yet reached the main sequence display near-IR excesses. Many of these are very faint optically and measured only in the near-IR.

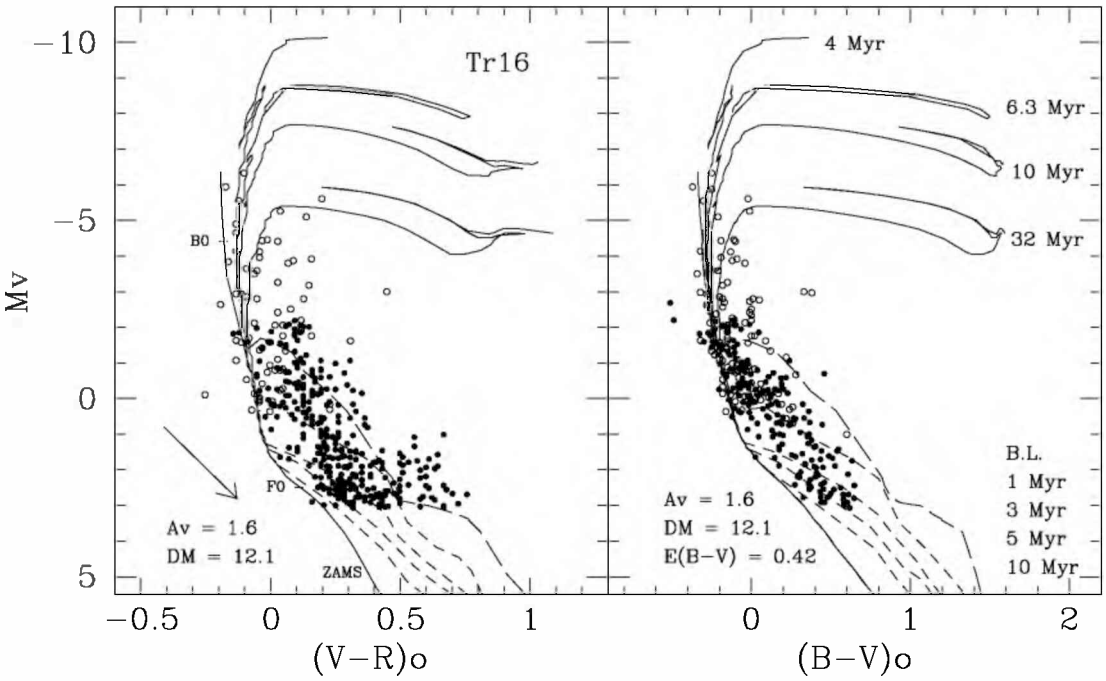

Figure 18. Calibrated colour-magnitude diagrams of Tr 16 at distance modulus (DM) and minimum extinction value A_V for stars with $V < 16.8$.

These will be the subject of a further study. On the other hand, a number of *K*-band bright stars in the field of Tr 14, namely IRS 71, IRS 81a and IRS 82, were classified as *K* and *M* giants by Smith (1987) based on low-resolution 2-μm band spectra. A few others, IRS 82, IRS 85 and IRS 89, have *JHK* colours of late-type evolved stars, some with slight IR excess. The 8.3-μm fluxes of IRS 81a and IRS 89 are above the *Midcourse Space Experiment* (*MSX*) detection limit at this wavelength. All these are most likely field giants, unrelated to Tr 14. Finally, several other mid-IR *MSX* (cf. Smith et al. 2000) compact and extended sources are located in the field of Tr 14. These are discussed in detail in Section 4.5.

4.4.3 Tr 16

The region occupied by this cluster seems to be the most complex in the Carina nebula. The apparently chaotic environment is caused by the violent interaction of the strong winds of the several O3 and WN stars, as well as from its most conspicuous member, η Carinae, with their surrounding medium; for recent reviews on η Carinae, see Gull, Johannson & Davidson (2001). This cluster is less compact than Tr 14 and the brightest stars are scattered over a large area with no defined nucleus.

The intracluster dust in this region shares the 'abnormal' characteristics of that in Tr 14 and Collinder 228 in the southern part of the great nebula (Feinstein et al. 1973; Tapia et al. 1988). The dust absorption across the cluster is very variable, showing the largest scatter in $E(V–J)$ and $E(B–V)$, although the mean extinction (median $E(J-K) = 5.7$) is lower than towards Tr 14 (Fig. 7 and Table 3). The implied small-scale inhomogeneities are corroborated by the presence of several dark cloudlets and atomic and molecular emission arcs and patches (Brooks et al. 2000; Rathborne et al. 2002). The interstellar dynamics is also extremely complex and beyond the scope of the present work.

The analysis of the *U–B* versus *B–V* diagram (Fig. 7) tells us that at these wavelengths the field star contamination is small and that all measured stars are A0 or earlier. A number of stars show peculiarly large $E(B-V)$ values: Tr 16–149, Tr 16–212, Tr 16–215, Tr 16–218, Tr 16–230, Tr 16–244 – identifications from Feinstein (1982). Not surprisingly, these are scattered around the 'keyhole' dark nebula and on the edge of the western 'dark lane'. A pair of stars on the eastern 'dark lane' also have extreme $E(B–V)$ and $E(B–U)$ values. Similarly to Tr 14, in the $E(B–V)$ versus $E(V–I)$ diagram (Fig. 8), the distinction between probable field stars and (anomalously reddened) members is quite straightforward. Again, most of the F0 and earlier stars appear to be associated with the cluster and those cooler are largely foreground objects. The few stars that show large colour excesses are near dark patches and the fraction of stars displaying near-IR excess seems to be similar to Tr 14 (Fig. 9), suggesting a similar age.

Fig. 18 shows another amazing feature not revealed before in any photometric work on Tr 16. At $0.5 \leqslant M_V \leqslant 2.5$, a 'strangulation' of the cluster main sequence takes place. Indeed, this is a case of low density of stars usually called a 'gap', a pattern that is even more clearly noticed in the $M_V/(V-R)_C$ diagram. Some authors argue that these 'gaps' (the so-called 'Böhm-Vitense gap'), already observed in other clusters among late-A and early-F stars, are the result of statistical fluctuations (e.g. Mazzei & Pigatto 1988). Others (e.g. Newberg & Yanny 1998; Rachford & Canterna 2000; Giorgi et al. 2002) give arguments against a statistical origin of such low star densities. However, their physical origin, if it does exist, is not known despite the attempts that have been made to relate them to the onset of surface convection zones (Böhm-Vitense & Canterna 1974; Rachford & Canterna 2000). Because dealing with these features is beyond the scope of the present work, we just point out that in the present case the gap appears near $(B–V) = 0.35$, close to the central value estimated for gaps in other well-studied samples of open clusters (Rachford & Canterna 2000). It should also be mentioned that the present gap is not an artefact produced by the manner in which we assessed cluster members in Tr 16, as we have included in Fig. 18 'all the stars' brighter than $M_V = 3$ found inside the cluster boundaries as determined in Section 4.1.

As in the case of Tr 14, it is impossible to interpret the upper part of the photometric HR diagram (Fig. 18) of Tr 16 because of the extremely variable extinction. As mentioned before, the reddening vector for bright members ($M_V < -1$) runs perpendicular to the isochrones for this cluster. It is only in the lower-luminosity part of the colour-magnitude diagram, where the reddening vector is parallel to the isochrones, that can we obtain a good estimate of the evolutionary phases which this cluster is going through. In fact, all massive stars with available slit spectroscopic classification can be dereddened to a position close to the zero-age main sequence (ZAMS), and, save for η Carinae, the only bright evolved star in the sample is HD 93162, a WN7 star.

Ignoring the stars located above the birthline, which statistically mostly belong to the field, the colour-magnitude diagrams (Fig. 18) for stars less massive than 4 $L_\odot$ suggest that the oldest members of Tr 16 are 3 to 6 million years old with no apparent limit to the youngest age. Therefore, we conclude that Tr 16 began the formation of stars of intermediate masses less than 6×10^6 yr ago and that it has probably been producing new stars in a continuous manner until recently. This result further supports the old suggestion that, historically, Tr 14 and Tr 16 started to be formed simultaneously out of a single parental cloud. It may be that, dynamically, their initial conditions would have led us to consider them a single cluster.

It must be added that we are also aware that part of the observed scatter in Tr 14 and Tr 16 for $M_V = 0$ can also be caused by a combination of photometric errors, differential reddening and perhaps a probable contribution of unresolved binaries among less massive stars (Preibisch & Zinnecker 1999; Hartigan, Strom & Strom 1994). In the context of our observations – present photometric limit of 'good data' – it is quite difficult to disentangle the binaries from the age spread but it is likely that all these effects acting together may contribute, at some extent, to increase the expected widening due to the 'true age spread'.

4.5 Active star formation towards Tr 14 and Car I

The properties of the clusters Tr 14, Tr 16 and Tr 15 provide elements to understand the star-formation history in the northern part of the Carina nebula up to probably the last 10^5 yr. It is also evident that the winds and UV radiation from the massive stellar population is interacting heavily with the remains of the molecular cloud from which the stars were formed. Nevertheless, these studies do not give clues as to whether or not stars presently continue to form in the complex.

Recent ^{12}CO mapping of the northern Carina nebula (Brooks et al. 1998) shows that the molecular emission is considerably clumpy and covers more than two degrees. The main CO hotspots coincide with parts of the V-shaped 'dark lanes' (Brooks et al. 1998, and references therein) and their mere existence hints that these regions may be presently active forming stars. Megeath et al. (1996) were the first to provide evidence of active star formation in the Carina nebula. They found a number of near-IR sources embedded in a 67-$M_\odot$ CO globule associated with *IRAS* 10430-5931. At the distance of NGC 3372, the total IR luminosity of the sources was found to be $L_{IR} > 10^4$ $L_\odot$, implying the presence of massive stars, although no radio H II regions have been detected in that direction. This region is located in the direction of an optically dark region some 8 arcmin to the southeast of η Carinae (i.e. the SE 'dark lane').

Two bright and large radio-continuum emission regions have been detected in the northern Carina nebula (Gardner et al. 1970; Whiteoak 1994; Brooks et al. 2001). These are called Car I and Car II. The latter, Car II, is located less than 2 arcmin to the NW of η Carinae. Its brightest features in the radio agree very well with those seen in the optical, including the well-known (though little understood) arc ('bubble-like') emission. On average, the ionized gas emission from Car II is lightly obscured by dust, although patchy obscuration is evident (Smith 2002). The gas is ionized by the numerous massive stars in Tr 16.

The northern bright ionized gas component Car I is, in striking contrast to the case of Car II, totally obscured by dense dust, coinciding with the NW 'dark lane'. The radio-continuum maps (Whiteoak 1994; Brooks et al. 2001) show a complex morphology. Two parallel ionization fronts have been identified. The faintest (Car I-E) coincides with the optical/near-IR arc of emission at the western edge of Tr 14 (see Section 4.1.2). A much brighter and sharper one (Car I-W) is located further to the west, marking the interface with the very dense molecular core, close to the CO emission peak, the latter totally devoid of radio-continuum emission. Several unresolved radio-emission knots are also located over the extended and faint emission plateau. Enough UV photons from the Tr 14 bright star members are available to excite externally the whole Car I H II region, and it has been assumed that no internal sources are present. Nevertheless, Brooks et al. (2001) suggested recently that the observed small radio-emission knots are compact (or ultracompact) H II regions, indicating the presence of massive very young stellar objects immersed in the cloud.

The idea of an embedded very young stellar population was given further evidence by Rathborne et al. (2002) who located a series of photodissociation regions (PDRs) by means of 3.3-μm SPIREX images. They matched these with *MSX* 8-μm maps to conclude that most of the diffuse emission at these wavelengths arises from polycyclic aromatic hydrocarbon (PAH) molecules in the PDRs. These authors pointed out that the lack of correlation, between the 8-μm (6.8 to 10.8 μm) and the 21-μm (18.2 to 25.1 μm) maps from *MSX* close to the position of the Car I-W ionization front and coincident with the CO peak, implies a very low thermal dust emission from this region. On the other hand, the 3.3-μm and 8-μm band emission is dominated by PAHs. Rathborne et al. (2002) also located four unresolved bright mid-IR sources in the area south of the nucleus of Tr 14, which they labelled N1, N2, N3 and N4. These were identified as very young O-type embedded stars.

The available CO emission maps of this region, although with low resolution (~40 arcsec), reveal a complex structure (Brooks et al. 1998). The cloud extends to the N, W and E of the main peak, even in the same direction as the bright visible nebula, implying that a large fraction of the molecular material is located *behind* the ionized gas and the optically visible Tr 14 cluster (cf. De Graauw et al. 1981). In fact, a fainter CO emission peak, at $\alpha = 10^h\ 43^m\ 55^s$, $\delta = -59^\circ\ 34'.7$ (J2000), coincides with a radio-continuum peak. This is within the area occupied by the cluster Tr 14. Based on our *UBVRIJHK* photometry (Section 4.1.2), there is no evidence that this molecular clump is located in front or mixed with the stars of the cluster. Rather, it confirms that the dense molecular gas, and the young stellar objects embedded in it, are *behind* Tr 14.

4.5.1 *IR sources behind Tr 14*

The present *JHK* images of the region give further information about the nature of the luminous young stellar objects N1, N2, N3 and N4 listed in table 4 of Rathborne et al. (2002).

The near-IR and mid-IR source N1 is bright in all *MSX* bands (cf. Smith et al. 2000) and the 3.3-μm, and presumably the 3.5-μm, emission is extended (Rathborne et al. 2002). N1 appears as a small nebulous object on our 2.2-μm image, reproduced in the upper right

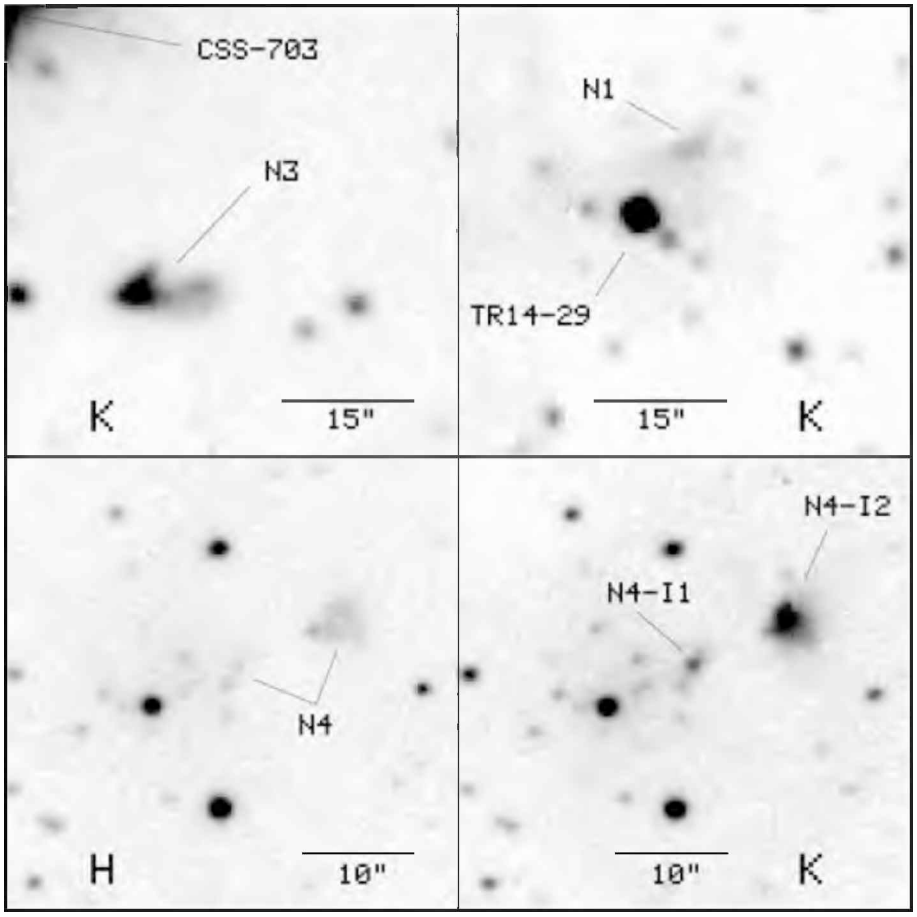

Figure 19. Near-IR images of the regions containing the mid-IR sources N1, N3 and N4 in the field of Tr 14 as discussed in Section 4.5.1. North is to the top, east to the left.

panel of Fig. 19. Its central coordinates are $\alpha = 10^{\rm h}\,43^{\rm m}\,04^{\rm s}3$, $\delta = -59^{\circ}\,33'\,35''$ (J2000) and its measured flux in the K-band is 16 mJy. This object is not seen on the 1.2- and 1.6-μm images. The spectral energy distribution (SED) and IR luminosity suggests that N1 is an embedded, recently born, O-type star (Rathborne et al. 2002) with a dust shell or disc at temperatures ranging from 87 to 330 K. As in similar cases, e.g. NGC 6334-I(North) (Megeath & Tieftrunk 1999), it is probable that the K-band emission knot is dominated by the H_2 2.12 line coming from shock-excited gas powered by mass outflows from a highly embedded (invisible at 2.2 μm) young stellar object. The bright star close to N1 is Tr 14-29, a moderately reddened B1.5 V member of the cluster. Although reported to be variable (cf. Feinstein et al. 1973), the range of magnitudes and colour indices measured at visible wavelengths for this star (VBFP; this work) are totally consistent with the characteristics of Tr 14 as discussed in Section 4.3.3. Unfortunately, the star saturates on our *JHK* images. There is no indication that this star is related to the IR source N1 which seems to be immersed in the dense molecular cloudlet behind Tr 14.

A very similar scenario is proposed for N3, a nebulous, double-peaked knot of emission at $\alpha = 10^{\rm h}\,43^{\rm m}\,11^{\rm s}2$, $\delta = -59^{\circ}\,37'\,13''$ (J2000) with a total 2.2-μm flux of 115 mJy (83 mJy from the eastern component and 32 mJy from the western component). This is the position of the 21-μm *MSX* peak. Again, we may be looking at shocked gas emission caused by an outflow from a massive object deep into the dense cloud. The IR luminosity of the embedded object is around $10^4\,L_{\odot}$ (Rathborne et al. 2002). The upper left panel of Fig. 19 shows the K-band image of this region. The extremely bright object just appearing at the northeast corner of the image is the S-type star CSS-703 (also known as Hen 4-100), first classified by G. Münch (Münch & Blanco 1955). This evolved star of uncertain mass, $\alpha = 10^{\rm h}\,43^{\rm m}\,13^{\rm s}3$, $\delta = -59^{\circ}\,36'\,37''$ (J2000), shows a moderate variability (a few tenths of a magnitude in K) with slight IR excess: $K \simeq 3.8$, $J - H \simeq 1.5$, $H - K \simeq 0.6$, $K - L \simeq 0.5$ (Feast, Catchpole & Glass 1976; Smith 1987; Van Eck et al. 2000). Catchpole & Feast (1976) suggested, based on the near coincidence of the radial velocities of the star and the Carina nebula, that this star may be a member of the Carina complex. This possible association would be difficult to reconcile with the ages derived for Tr 14. The flux from the S star at 8 μm is considerably higher than that from the nebulous object N3, but at $\lambda > 11$ μm the emission from the embedded young stellar object dominates. In fact, the *MSX* 8-μm map shows the main peak at the position of the S star and a secondary peak at the position of the nebulosity. The *MSX* catalogue lists both these peaks as a single entry. This confusion led Rathborne et al. (2002) to propose a two component (2500 K photosphere plus 100 K envelope) emission of a single object to explain its SED. The fact is that the two sources are separated by 29 arcsec. The photosphere of the cool and evolved star CSS-703 shows a blackbody at a temperature of around 1900 K while N3 shows a SED similar to the other young stellar objects in the region.

The near-IR morphology of the mid-IR source N4, with 2.2-μm peak emission at $\alpha = 10^{\rm h}\,43^{\rm m}\,30^{\rm s}8$, $\delta = -59^{\circ}\,33'\,11''$ (J2000) is somewhat more complex. The bottom panels of Fig. 19 show the H

and *K* images of this region. Because this field is close to Tr 16, our near-IR images were secured with the 2.5-m telescope, resulting in deeper images than those for the Tr 14 field (taken with the 1.0-m telescope). Very close to the *MSX* peak position, faint diffuse emission at 1.6 and 2.2 μm is seen covering an area of some 15 × 15 arcsec^2. On top of this, an unresolved source, labelled N4-I1 in Fig. 19 and located at the position $\alpha = 10^{\rm h}\,43^{\rm m}\,32^{\rm s}.1$, $\delta = -59^\circ\,33'\,16''$ (J2000), is seen only in the 2.2-μm image with $K = 12.22$ and $H{-}K \geqslant 2.2$. A second, extended near-IR source of radius ~4 arcsec, N4-I2, is located at $\alpha = 10^{\rm h}\,43^{\rm m}\,30^{\rm s}.8$, $\delta = -59^\circ\,33'\,11''$ (J2000). This source is detected also at 1.6 μm and its photometry yielded $K = 10.91$, $H{-}K = 2.22$ and $J{-}H > 2.2$. From the IR luminosity of the object, Rathborne et al. (2002) inferred the presence of an embedded O9 star. It may be that N4-I1 is the photosphere of this star (reddened by $A_V \sim 40$). On the other hand, the observed flux in the *K* and *H* bands from the nebulous N4-I2 may again be dominated by H_2 and [Fe II] shocked gas emission, respectively.

Finally, the mid-IR source N2, the coolest of those reported by Rathborne et al. (2002), was not detected in any of our images. In conclusion, the present near-IR images provide further evidence of recent star formation in the dense molecular cloud behind the optical Tr 14 cluster/nebula complex.

4.5.2 IR sources in Car I

The suggestion of the existence of a very young stellar population closer to the densest and more massive molecular clump associated with the radio H II region Car I was tested by means of deep near-IR images taken with the 2.5-m DuPont telescope at Las Campanas. A field of size 82 × 86 arcsec^2, centred close to the peak radio emission of Car I, was imaged in the *JHK* bands. The 2.2-μm frame is shown in Fig. 20. 33 sources with $K < 17$ were located and measured photometrically, though 11 were not detected at wavelengths shorter than 2 μm. Fig. 21 shows the *J–H* versus *H–K* diagram of the sources detected in the three colours in this field together with the *K* versus *H–K* diagram of those detected in *H* and *K*.

Most of the brightest stars have *JHK* colours of foreground stars (encircled in Fig. 20). There are 19 sources with $K \leqslant 15$ which, judging from the near-IR colours, may be associated with the dense cloud. These are listed, with coordinates and photometry, in Table 4. None was detected in *J* and nine were fainter than our detection limit in *H*. With only three exceptions (discussed below), all these sources are within the diffuse 2.2-μm boomerang-shaped diffuse emission. This extended emission is present in the three *JHK* frames, implying a reflection origin. Logically, we can infer that most of the faint IR sources in the area are illuminating the dust of the cloud and thus immersed in it. The colour-magnitude diagram (Fig. 21) shows that at least three of them are highly reddened ($A_V > 25$) B stars, while most probably several of those with $H > 17.5$ (undetected by us) are probably embedded deep in the cloud. Of particular importance is source 21, located within 2 arcsec of the position of an ultracompact H II region ('compact source') discovered by Brooks et al. (2001). It requires an O9.5 V ionizing star and this is totally consistent with the present photometry of source 21 and its 3.3-μm counterpart. Sharing very similar photometric characteristics is source 2, located close to the southern edge of our image. Its position is just outside the diffuse emission and there does not seem to be any associated feature in the radio maps. This source is embedded in the diffuse 3.3- and 8-μm emission, Car I-W, thought to originate from PAHs and marking a further ionization front (Brooks et al. 2001).

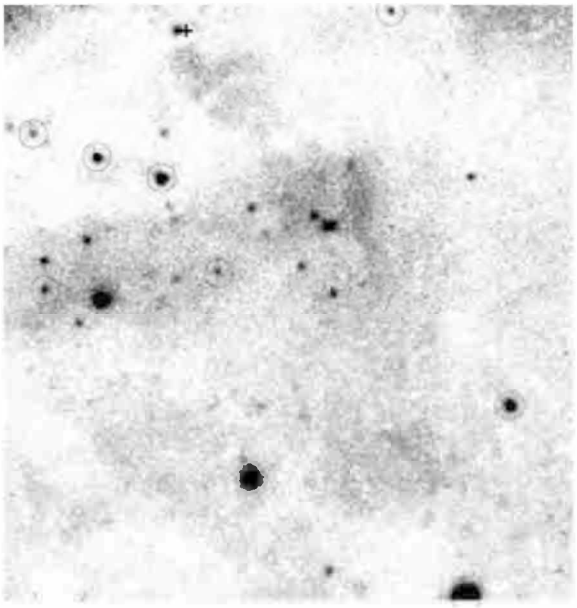

Figure 20. *K*-band long-exposure image of the Car I region. The area covered is 82 × 86 arcsec^2 centred at $\alpha = 10^{\rm h}\,43^{\rm m}\,22^{\rm s}.6$; $\delta = -59^\circ\,34'\,40''$ (J2000). The plus sign marks the position of the compact H II region reported by Brooks et al. (2001). Stars that have *JHK* colours indicative of being in the foreground are marked with circles. North is to the top, east to the left.

These new detections confirm the idea that a new generation of stars is being born at the ionization fronts which are the present interactions of the extreme UV field provided by Tr 14 with the densest molecular clumps behind and to the west of the visible cluster.

5 CONCLUSIONS

The main results of the optical and near-IR photometric imaging study of more than 832 arcmin^2 of the northern Carina nebula are listed below.

(1) Based on star counts in the magnitude range $11.5 < V < 18$, the centres and extensions of the clusters Tr 14 ($r = 264$ arcsec), Tr 15 ($r = 320$ arcsec) and Tr 16 ($r = 320$ arcsec) were determined. It was confirmed that Cr 232 is not a true cluster but a condensation of bright stars originally belonging to Tr 14 or Tr 16. The distribution of stars in Tr 14 in the near-IR, which maps deeper into the obscuring material, differs from that at visible wavelengths. At 1.6 and 2.2 μm, Tr 14 appears to have a nucleus of radius 100 arcsec with a 120-arcsec extension towards the SW ending abruptly at the edge of a dense molecular clump.

(2) The widespread variations in dust density and also in dust size distribution leading to widely different values of A_V and reddening laws towards Tr 14 and Tr 16 are confirmed. No spatial patterns were found for these variations.

(3) Using the derived values of the colour excess index $E(V{-}J)$ for the cluster members with reliable two-dimensional slit spectral classifications from the literature together with recent absolute magnitude calibrations, new extinction values and distances to Tr 14, Tr 15 and Tr 16 were obtained. These are consistent with all three clusters being at a similar distance from the Sun ($\langle {\rm DM} \rangle = 12.14$) but the data have shown very large scatter in both A_V and *d*, which may be real and not caused by observational errors. Large dust inhomogeneities cause the extinction to be highly variable, even within individual clusters.

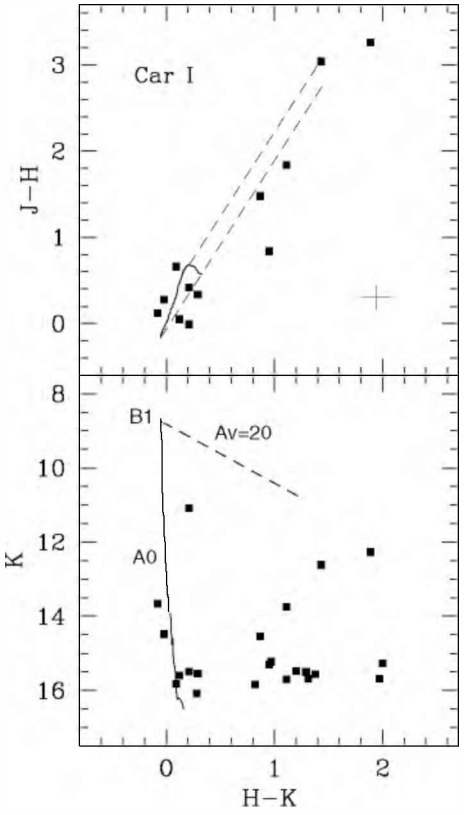

Figure 21. Upper panel: *J–H* versus *H–K* diagram of the sources in the field of Car I shown in Fig. 20. The continuous line represents the locus occupied by unreddened main-sequence stars. The two parallel dashed lines represent the standard reddening vectors (of length $A_V = 20$) for late-type and early-type stars. The cross indicates the maximum photometric errors. Lower panel: *K* versus *H–K* diagram for the sources in the field of Car I. The continuous line represents the locus of the main sequence at distance modulus 12.1 and no extinction. The two parallel dashed lines represent the standard reddening vectors.

Table 4. *HK* photometry of the sources possibly associated with Car I.

No	RA h m s (J2000)	Dec.	*K*	*H–K*
2	10 43 24.7	−59 34 00	15.3	>2.2
6	10 43 26.7	−59 34 42	15.68	1.95
8	10 43 21.7	−59 34 38	15.51	1.27
11	10 43 22.3	−59 34 34	15.7	1.09
12	10 43 27.3	−59 34 33	15.31	0.93
13	10 43 26.5	−59 34 30	15.23	0.95
15	10 43 22.1	−59 34 27	15.27	1.98
16	10 43 23.3	−59 34 26	15.57	1.46
18	10 43 19.1	−59 34 21	15.48	1.18
21	10 43 21.8	−59 34 18	14.97	>2.5
25	10 43 24.7	−59 34 36	16.11	>1.4
26	10 43 23.0	−59 34 29	16.48	>1.0
27	10 43 24.8	−59 34 27	16.05	>1.5
28	10 43 24.9	−59 34 25	16.83	>0.8
29	10 43 25.2	−59 34 35	16.1	>1.4
30	10 43 25.0	−59 34 39	16.16	>1.3
31	10 43 22.3	−59 34 56	16.2	>1.3
32	10 43 21.4	−59 34 19	15.84	0.80
33	10 43 25.0	−59 34 14	15.68	1.29

(4) The northernmost cluster, Tr 15, is the least reddened and apparently away from dense molecular material, although a few of its individual members (notably Tr 15–18) suffer from a much higher extinction, probably of circumstellar origin. It contains a few blue supergiants and maybe one or two red supergiants. No evidence was found for the existence of other stars with IR excesses in the cluster. The intrinsic colour-magnitude diagram of Tr 15 suggests that the stars of this cluster have ages between 3 and 40 million years.

(5) The present optical and near-IR photometry coupled with CO data indicates that Tr 14, the richest and most highly concentrated cluster of the Carina nebula, is partially embedded in a dense molecular clump located behind the optical nebulosity. This causes the photometry of the cluster to be less contaminated by background stars, a characteristic that is shared with Tr 16 and consistent with the two-colour diagrams of both clusters. Additionally, the sharp south-western boundaries of the Tr 14 cluster are delineated by an ionizing front caused by the expansion of the H II region into the dense molecular cloud. This is seen as an arc of emission in the optical, IR and radio contouring a very dark cloud. Several low luminosity stars in the cluster show 2.2-μm excesses, indicating the possible presence of discs around them. The highly inhomogeneous dust in the environment of Tr 14 makes the interpretation of the colour-magnitude diagram of the cluster very complicated, in particular for the stars with no spectroscopic classification. Nevertheless, the data seem to suggest that the formation of Tr 14 stars of *all* masses (down to our limit of 2 $M_\odot$) started 5×10^6 yr ago, proceeding continuously until less than one million years ago.

(6) The complex morphology of the Tr 16 region is caused by the violent interaction of the strong winds and explosions of its most conspicuous members, η Carinae and other highly luminous stars, with their surrounding medium. Nevertheless, the optical and near-IR photometric properties of its stellar population seem to be similar to those of Tr 14 except for the presence of the evolved objects HD 93162 (WN7) and η Carinae. The calibrated colour-magnitude diagrams of Tr 16 are compatible with ages between less than one and six million years.

(7) Deep *JHK* images of the region centred on the radio H II region with no optical counterpart Car I reveal the presence of an embedded stellar population which includes at least one O9–B0 star with an ultracompact H II region associated. A number of very red fainter sources have no compact radio-continuum counterparts. All IR sources probably associated with the region are located within an extended IR V-shaped reflection nebula with one of its arms coinciding with a photodissociation region characterized by 3.3- and 8-μm emission.

(8) The presence of 2.2-μm nebulous emission is reported at the position of three mid-IR sources (N1, N3 and N4) previously reported in the area of Tr 14. These are assumed to be dominated by molecular hydrogen 2.12-μm emission emitted by shocked gas powered by embedded massive young stellar objects. Arguments are given that support the idea that these objects and the dense molecular clump are located behind the optical nebula and the cluster Tr 14.

ACKNOWLEDGMENTS

We thank the staff of Las Campanas Observatory for their support. Part of this work was financially supported by DGAPA–UNAM grant No IN-105400 (MT). MT acknowledges the hospitality of Dr Giovanni Fazio and the Harvard–Smithsonian Center for Astrophysics where he enjoyed an SAO short-term visiting appointment during which part of this manuscript was prepared. We also thank

Dr Nolan Walborn for comments and suggestions that helped to improve the content of this paper.

REFERENCES

Bohigas J., Tapia M., Ruiz M. T., Roth M., 2000, MNRAS, 312, 295
Böhm-Vitense E., Canterna R., 1974, ApJ, 194, 629
Bressan A., Fagotto F., Bertelli G., Chiosi C., 1993, A&AS, 100, 647
Brooks K. J., Burton M. G., Rathborne J. M., Ashley M. C. B., Storey J. W. V., 2000, MNRAS, 319, 95
Brooks K. J., Whiteoak J. B. Z, Storey J. W. V., 1998, PASAust, 15, 202
Brooks K. J., Storey J. W. V., Whiteoak J. B., 2001, MNRAS, 327, 46
Carraro G., 2002, MNRAS, 331, 785
Catchpole R., Feast M. W., 1976, MNRAS, 175, 501
Cox P., 1995, in Niemela V., Morrell N., Feinstein A., eds, The η Carinae region: a laboratory of stellar evolution. RevMexAA Conf. Ser., 2, 105
Cudworth K. M., Martin S. C., DeGioia-Eastwood K., 1993, AJ, 105, 1822
DeGioia-Eastwood K., Throop H., Walker G., Cudworth K. M., 2001, ApJ, 549, 578 (DTWC)
De Graauw T., Lidholm S., Fitton B., Beckman J., Israel F. P., Nieuwenhuijzen H., Vermue J., 1981, A&A, 102, 257
Feast M. W., Catchpole R., Glass I. S., 1976, MNRAS, 174, 81
Feinstein A., 1982, AJ, 87, 1012
Feinstein A., 1995, in Niemela V., Morrell N., Feinstein A., eds, The η Carinae region: a laboratory of stellar evolution. RevMexAA Conf. Ser., 2, 57
Feinstein A., FitzGerald P. M., Moffat A. F. J., 1980, AJ, 85, 708
Feinstein A., Marraco H. G., Muzzio J. C., 1973, A&AS, 12, 331
García B., Walborn N. R., 2000, PASP, 112, 1549
García B., Malaroda S., Levato H., Morrell N., Grosso M., 1998, PASP, 110, 53
Gardner F. F., Milne D. K., Metzger P. G., Wilson, T. L., 1970, A&A, 7, 349
Giorgi E., Vázquez R. A., Baume G., Seggewiss J.-M., Will J.-M., 2002, A&A, 381, 884
Gull T. R., Johannson S., Davidson K., 2001, ASP Conf. Ser. Vol. 242. Astron. Soc. Pac., San Francisco, p. 1
Hartigan P., Strom K. M., Strom S., 1994, ApJ, 427, 961
Herbst W., 1976, ApJ, 208, 923
Jones T. J., Ashley M., Hyland A. R., Ruelas-Mayorga A., 1981, MNRAS, 197, 413
Johnson H. L., Morgan W. W., 1953, ApJ, 117, 313
Kaltcheva N. T., Georgiev L. N., 1993, MNRAS, 261, 847
Kenyon S., Hartmann L., 1995, ApJS, 101, 117
Koornneef J., 1983, A&A, 128, 84
Lee D.-H., Min K.-W, Dixon W. V. D., Hurwitz M., Ryu K.-S., Seon K.-I., Edelstein J., 2000, ApJ, 545, 885
Levato H., Malaroda S., 1981, PASP, 93, 714
Levato H., Malaroda S., 1982, PASP, 94, 807
Levato H., Malaroda S., Morrell N., García B., Hernández C., 1991, ApJS, 75, 869
Levato H., Malaroda S., Morrell N., García B., Grosso M., 2000, PASP, 112, 359
Massey P., Johnson J., 1993, AJ, 105, 980 (MJ)
Mazzei P., Pigatto L., 1988, A&A, 193, 148
Megeath S. T., Tieftrunk A. R., 1999, ApJ, 526, 113
Megeath S. T., Cox P., Bronfman L., Roelfsema P. R., 1996, A&A, 305, 296
Morrell N., García B., Levato H., 1988, PASP, 100, 1431
Munch G., Blanco V. M., 1955, AJ, 60, 154
Newberg H. J., Yanny B., 1998, ApJ, 499, L57
Palla F., Stahler S. W., 1999, ApJ, 525, 771
Persson S. E., West S. C., Carr D. M., Sivaramakrishnan A., Murph D. C., 1992, PASP, 104, 204
Preibisch T., Zinnecker H., 1999, AJ, 117, 2381
Rachford B. L., Canterna R., 2000, AJ, 119, 1302
Rathborne J. M., Burton M. G., Brooks K. J., Cohen M., Ashley M. C. B., Storey J. W. V., 2002, MNRAS, 331, 85
Schmidt-Kaler Th., 1983, in Schaifers K., Voight H. H., eds, Landolt-Börnstein, Neue Ser., p. 1, Gr VI, Vol. 2b, Stars and Star Clusters. Springer, Berlin, p. 10
Smith R. G., 1987, MNRAS, 227, 943
Smith N., 2002, MNRAS, 331, 7
Smith N., Egan M. P., Carey S., Price D., Morse J. A., Price P. A., 2000, ApJ, 532, L148
Stetson P. B., 1987, PASP, 99, 191
Tapia M., 1995, in Niemela V., Morrell N., Feinstein A., eds, The η Carinae region: a laboratory of stellar evolution. RevMexAA Conf. Ser., 2, 87
Tapia M., Roth M., Marraco H., Ruiz M. T., 1988, MNRAS, 232, 661
Thé P. S., Graafland F., 1995, in Niemela V., Morrell N., Feinstein A., eds, The η Carinae region: a laboratory of stellar evolution. RevMexAA Conf. Ser., 2, 75
Tovmassian H. M., 1995, in Niemela V., Morrell N., Feinstein A., eds, The η Carinae region: a laboratory of stellar evolution. RevMexAA Conf. Ser., 2, 83
Turner D. G., Moffat A. F. J., 1980, MNRAS, 192, 283
Vacca W. D, Garmany C. D., Shull M., 1996, ApJ, 460, 914
Van Eck S., Jorissen A., Udry S., Mayor M., Burki G., Burnet M., Catchpole R., 2000, A&AS, 145, 51
Vázquez R. A., Baume G., Feinstein A., Prado P., 1996, A&AS, 116, 75 (VBFP)
Walborn N. R., 1973, ApJ, 179, 517
Walborn N. R., 1982, AJ, 87, 1300
Walborn N. R., 1995, in Niemela V., Morrell N., Feinstein A., eds, The η Carinae region: a laboratory of stellar evolution. RevMexAA Conf. Ser., 2, 51
Walborn et al., 2002, AJ, 123, 2754
Whiteoak J. B. Z., 1994, ApJ, 429, 225
Whiteoak J. B. Z., Otrupcek R. E., 1984, Proc. Astron. Soc. Aust. 5(4), 552

This paper has been typeset from a TEX/LATEX file prepared by the author.